Alexandria Engineering Journal (2016) 55, 169–186

HOSTED BY

Alexandria University

Alexandria Engineering Journal

www.elsevier.com/locate/aej
www.sciencedirect.com

ORIGINAL ARTICLE

Heatline visualization of natural convection heat transfer in an inclined wavy cavities filled with nanofluids and subjected to a discrete isoflux heating from its left sidewall

Ahmed Kadhim Hussein [a], **Salam Hadi Hussain** [b,*]

[a] *Department of Mechanical Engineering, College of Engineering, Babylon University, Babylon Province, Iraq*
[b] *Department of Automobile Engineering, College of Engineering-Al Musayab, Babylon University, Iraq*

Received 23 October 2015; revised 5 December 2015; accepted 20 December 2015
Available online 9 January 2016

KEYWORDS

Heatline visualization;
Natural convection;
Isoflux heating;
Nanofluid;
Wavy cavity

Abstract Natural convection visualization by heatlines in three types of inclined wavy cavities filled with Al_2O_3–water and Ag–water nanofluids and subjected to a discrete isoflux heating from its left sidewall is investigated numerically in this work. The right sidewall together with remaining regions in the left sidewall is insulated. The solution is based on the finite volume method. The upper and lower cavity walls are maintained at a constant cold temperature and follow a profile of sine wave. Numerical computations are carried out for various values of the solid volume fraction [φ = 0, 0.05, 0.1, 0.15 and 0.2], number of undulations [N = 1, 2 and 3], Rayleigh number [Ra = 10^3–10^7], the ratio of heating element length to the cavity height [ε = 0.2, 0.4, 0.6, 0.8 and 1.0], the cavity inclination angle [Φ = 0°, 30°, 60° and 90°] and the wave amplitude [γ = 0.1, 0.15 and 0.2]. The results are presented in terms of heatlines, isotherms, streamlines together with local and average Nusselt numbers. It is found that the geometry of the wavy cavity has a cursive role on the flow and thermal fields pattern. The results also explained that streamlines and isotherms were affected significantly for high Rayleigh number and vertical cavity position [Φ = 90°]. Also, when the solid volume fractions and wave amplitudes increase, the local Nusselt number along the heat source increases. Furthermore, velocity profiles increase as [ε] increases near the left sidewall of the cavity while they decrease as [ε] increases near the right sidewall of the cavity. For all three types of horizontal wavy cavities the heat functions increase for both nano and base fluids when the wave amplitude increases. Finally, results of the present work indicated that both heatlines and heat functions techniques are applied efficiently to describe the natural convection heat transfer inside wavy cavities filled with nanofluid.

* Corresponding author.
E-mail addresses: ahmedkadhim7474@gmail.com (A.K. Hussein), salamphd1974@yahoo.com, met.salam.hadi@uobabylon.edu.iq (S.H. Hussain).

Peer review under responsibility of Faculty of Engineering, Alexandria University.

http://dx.doi.org/10.1016/j.aej.2015.12.014
1110-0168 © 2015 Faculty of Engineering, Alexandria University. Production and hosting by Elsevier B.V.

Nomenclature

C_p	specific heat at constant pressure (kJ/kg K)
g	gravitational acceleration (m/s^2)
k	thermal conductivity (W/m K)
L	height or Width of the corrugated enclosure (m)
P	dimensionless pressure
p	pressure (Pa)
Pr	Prandtl number (v_f/α_f)
q''	heat flux (W/m^2)
Ra	Rayleigh number($g\beta_f L^3\Delta T/v_f\alpha_f$)
T	temperature (K)
T_c	temperature of the cold surface (K)
N	number of undulations
Nu^s	local Nusselt number on the heat source surface
$\overline{\mathrm{Nu}_s}$	average Nusselt number along the heat source
U	dimensionless velocity component in x-direction
u	velocity component in x-direction (m/s)
V	dimensionless velocity component in y-direction
v	velocity component in y-direction (m/s)
X	dimensionless coordinate in horizontal direction
x	Cartesian coordinate in horizontal direction (m)
Y	dimensionless coordinate in vertical direction
y	Cartesian coordinate in vertical direction (m)

Greek symbols

α	thermal diffusivity (m^2/s)
θ	dimensionless temperature (T $- T_c/\Delta T$)
γ	sinusoidal wave amplitude (m)
Ψ	dimensional stream function (m^2/s)
ψ	dimensionless stream function
μ	dynamic viscosity (kg s/m)
v	kinematic viscosity (μ/ρ)(Pa s)
ε	ratio of heating element length to the enclosure height (%)
φ	nanoparticle volume fraction (%)
Φ	enclosure inclination angle with X-axis (degree)
ΔT	ref. temperature difference (q'' L/k_f)
β	volumetric coefficient of thermal expansion (K^{-1})
ρ	density (kg/m^3)
Π	heat function

Subscripts

c	cold
f	fluid (pure)
P	nanoparticle
nf	nanofluid
s	source surface

Abbreviations

Min	minimum
b	base heat source
max	maximum
v	vertical heat source

1. Introduction

Nano is a Greek word which means 'dwarf'. In recent times, nanofluids are used in huge industrial applications such as construction, nuclear reactor coolant, solar cells, oil industry, electronics, renewable energy and many others [1–4]. The reason of these huge applications of nanofluid can be go back to its high thermal conductivity compared with traditional fluids such as oil, toluene and water. Nanofluids can be defined as fluid suspensions of nanoparticles with at least one of their dimensions smaller than 100 nm [5–8]. For more comprehensive details about nanofluids and their applications, the reader can go to the excellent review papers by Murshed et al. [9], Wang and Quintard [10] and Saidur et al. [11]. Natural convection or sometimes called buoyancy-driven convection takes an increasing area of interest by numerous researchers due to its importance in many significant fields such as micro-electronics industry, lubrication systems, energy efficient of buildings and fire control. Natural convection in cavities of classical geometry filled with traditional fluids is considered by many authors such as Calcagni et al. [12], Hussain and Hussein [13] and Khezzar et al. [14]. While, Kolsi et al. [15], He et al. [16] and Sheikhzadeh et al. [17] studied it in classical cavities filled with a nanofluid. However, in many practical and industrial applications the cavities are strongly shifted from classical geometry such as in solar collectors, food industries, heat exchangers, fuel cell technology and microelectronic equipments. One of the most important irregular geometries of cavities is the wavy geometry. Numerous researchers studied the natural convection in wavy cavities filled with classical fluids under different boundary conditions. Mahmud et al. [18] investigated numerically the natural convection in an enclosure with vertical wavy walls and two insulated horizontal walls. They concluded that the heat transfer was highly enhanced when the enclosure aspect ratio was considered low. Adjlout et al. [19] studied numerically the effect of a hot wavy wall of a laminar natural convection in an inclined differentially heated cavity. Two geometrical configurations were considered with one and three undulations. The results obtained showed that the hot wall undulation affected the flow and the heat transfer rate in the cavity. Das et al. [20] studied the effect of surface waviness and aspect ratio on heat transfer inside a wavy enclosure. The top and bottom walls were considered wavy and isothermal, while, two straight-vertical sidewalls were considered adiabatic. Simulation was carried out for a range of surface waviness ratios [λ = 0–0.25], aspect ratios [A = 0.25–0.5] and Rayleigh numbers [Ra = 10^6–10^7] for a fluid having Prandtl number equals to 1.0. They suggested that the natural convection was changed considerably when surface waviness changed and also depended on the aspect ratio of the domain. Mushatet [21] simulated numerically the natural convection inside an inclined differentially heated square cavity with two vertical wavy walls. The top and bottom walls were adiabatic. A curvilinear coordinate generation system was used to transfer a physical space into a computational one. The effect of inclination angle, amplitude and number of undulations on heat transfer and fluid flow was investigated for Ra = 10^5. The results showed that the increase of the cavity amplitude led to decrease the local Nusselt number. Bendehina et al. [22] studied the influence of non-uniform boundary conditions on the natural

convection in inclined differentially heated cavities. The hot wall was considered wavy with three undulations. The aspect ratio of the cavities was changed and various inclination angles were performed. The results showed that the trend of the local Nusselt number was wavy for all inclination angles. More research papers related with the natural convection in a wavy cavity filled with traditional fluid can be found in [23–27]. From the other side, researches involved the natural convection in a wavy cavity filled with nanofluid are still limited. Chang Cho et al. [28] studied the natural convection heat transfer characteristics within an enclosed wavy cavity filled with nanofluid. The complex-wavy-surface was modeled as a superimposition of two sinusoidal functions. They concluded that the heat transfer performance was optimized by tuning the wavy-surface geometry parameters in accordance with the Rayleigh number. Nikfar and Mahmoodi [29] investigated numerically using the meshless local Petrov–Galerkin method, the natural convection of Al_2O_3–water nanofluid in a cavity with wavy sidewalls. The horizontal top and bottom walls of the cavity were kept insulated. Two different models were considered for the effective dynamic viscosity of the nanofluid. They concluded that the average Nusselt number estimated for Brinkman formula increased with the increase in volume fraction of the nanoparticles while it decreased for Maiga's correlation. Esmaeilpour and Abdollahzadeh [30] analyzed using a finite-volume numerical procedure, the free convection and entropy generation of a nanofluid inside an enclosure with different patterns of vertical wavy walls. The results indicated that the average Nusselt number decreased nearly linear with the increase of solid volume fraction. They concluded that the entropy generation increased with increasing the Grashof number and decreased with increasing the surface waviness. Chang Cho et al. [31] simulated numerically the natural convection in a wavy-wall enclosure filled with Cu–water nanofluid. The bottom wall of the enclosure had a wavy geometry and was maintained at a constant high temperature, while the top one was straight and maintained at a constant low temperature. The left and right sidewalls were considered straight and insulated. They examined the effect of the nanoparticle volume fraction, Rayleigh number, the wave amplitude, and the wavelength on the heat transfer characteristics. It was shown that the heat transfer performance could be enhanced as the volume fraction of nanoparticles increased. Recently, Mansour and Bakier [32] investigated numerically the free convection in a complex-wavy-wall cavity filled with nanofluid. The left and right sidewalls of the cavity had a complex-wavy geometry and maintained at low and high temperatures, respectively, while, the upper and lower walls of it were considered flat and adiabatic. The nanofluid was composed of Al_2O_3 nanoparticles suspended in pure water. They examined the effects of the solid volume fraction, the Rayleigh number and the geometry parameters on the streamlines, isotherm and Nusselt number in the cavity. The results showed that the Nusselt number, increased as the solid volume fraction increased. Further references can be found in [33,34].

Recently, more attention was focused to notice the heat transfer path inside enclosures especially for convection heat transfer problems. Unfortunately, the classical method of heat flow visualization by isotherms does not offer this important observation. For this reason, the so-called heatline visualization technique which was suggested by Kimura and Bejan [35] was used efficiently in recent years to solve this problem. Costa [36] in his excellent review paper about heatlines referred that, the numerical values of the dimensionless heat function were closely related to the average Nusselt number. They were considered a very efficient tool to visualize and analyze the convection heat transfer process. Oztop et al. [37] performed a heatline analysis of natural convection in a square inclined enclosure filled with a CuO nanofluid under a non-uniform wall heating condition from a wall and cooled from opposite wall, while other walls were adiabatic. Calculations were performed for Rayleigh numbers of $[10^3 \leqslant Ra \leqslant 105]$, inclination angle of $[0° \leqslant \phi \leqslant 90°]$ and nanoparticle fraction of $[0 \leqslant \varphi \leqslant 0.1]$. It was observed that heat transfer in the cavity increased by adding nanoparticles. Visualization of heatline was successfully applied to nanoparticle convective flows. Basak and Chamkha [38] investigated numerically based on heat flow visualization by heat functions or heatlines the natural convection of various nanofluids [copper–water, alumina–water and TiO_2–water] in the presence of hot and cold sidewalls (case 1) or uniform or non-uniform heating of bottom wall with cold sidewalls (case 2). It was found that heatlines with larger heat functions values for nanofluids coincided with heatlines with smaller heat function values for water at walls.

From the above peer literature survey and based upon our experience, there is no paper up to date deals with the natural convection visualization by heatlines in an inclined wavy cavity of different geometries filled with nanofluids and subjected to a discrete isoflux heating from its left sidewall. Also, there is no study in the literature determined the heat function for nanofluid inside classical or wavy cavities with presence of isoflux boundary condition. Therefore; in our opinion this work gives an original contribution in this significant field.

2. Problem formulation and the mathematical model

The configuration which was considered in the present work is illustrated in Fig. 1. Three types of two-dimensional wavy cavity of height and width (L) are considered as shown in Fig. 1. These types are represented as types I, II and III for clarity. Both upper and lower walls of cavities are considered wavy and maintained at an isothermal cold temperature (T_c). Some regions in the straight left sidewall for all cavities are subjected to a discrete isoflux heating, while the other regions of this wall together with straight right sidewall are considered adiabatic. All cavities are filled with Al_2O_3–water or Ag–water nanofluids. The fluid flow inside cavities is assumed to be Newtonian, laminar and time-independent. The Al_2O_3 and Ag nanoparticles are assumed in a thermal equilibrium with the base fluid (i.e., water) while the slipping between them is assumed negligible. Moreover, all the physical properties of both base fluid and nanoparticles are assumed invariant with temperature except the density which was treated according to Boussinesq's approximation. The thermo-physical properties of the water, sliver (Ag) and Alumina (Al_2O_3) are given in Table 1 as given by Aminossadati and Ghasemi [39]. The solid volume fraction (φ) is varied as [φ = 0, 0.05, 0.1, 0.15 and 0.2] while the number of undulations is varied as [N = 1, 2 and 3]. The Rayleigh number range is [$Ra = 10^3$–10^7], the ratio of heating element length to the cavity height (ε) is varied as [ε = 0.2, 0.4, 0.6, 0.8 and 1.0], the cavity inclination angle which is measured with X-axis (Φ) is varied as [Φ = 0°, 30°, 60° and 90°] and

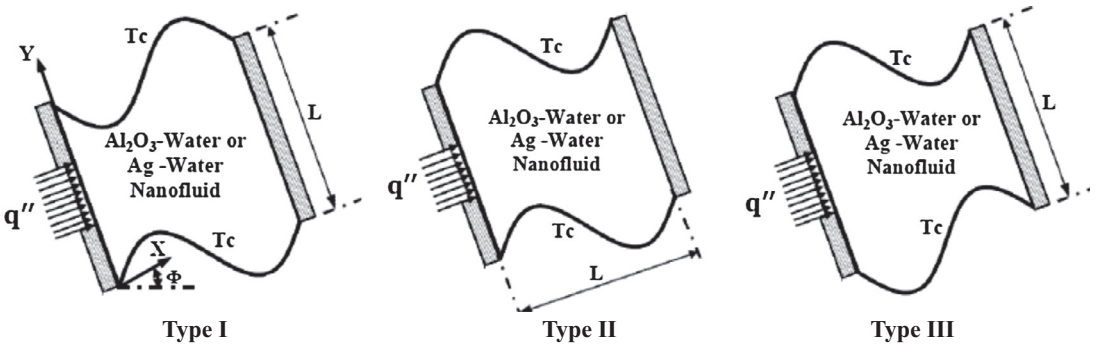

Figure 1 Physical domain for three types of wavy cavity along with boundary conditions.

Table 1 Thermo-physical properties of base fluid (pure water) and nanoparticles [39].

Properties	Pure water	Silver (Ag)	Alumina (Al_2O_3)
Cp (J/kg K)	4179	235	765
K (W/m K)	0.613	429	40
ρ (kg/m^3)	997.1	10,500	3970
β (1/K) $\times 10^5$	21	1.89	0.85

the sinusoidal wave amplitude is varied as [γ = 0.1, 0.15 and 0.2]. The dimensionless mass, momentum and energy equations for the natural convection fluid flow and heat transfer in the considered wavy cavities can be obtained by utilizing the following dimensionless quantities:

$$X=\frac{x}{L},\ Y=\frac{y}{L},\ U=\frac{uL}{\alpha_f},\ V=\frac{vL}{\alpha_f},\ P=\frac{pL^2}{\rho_{nf}\alpha_f^2},$$

$$\theta=\frac{T-T_c}{\Delta T},\ \Delta T=\frac{q''L}{k_f},\ \mathrm{Ra}=\frac{g\beta_f L^3\Delta T}{\nu_f\alpha_f},\ \mathrm{Pr}=\frac{\nu_f}{\alpha_f}$$

$$\frac{\partial U}{\partial X}+\frac{\partial V}{\partial Y}=0 \tag{1}$$

$$U\frac{\partial U}{\partial X}+V\frac{\partial U}{\partial Y}=-\frac{\partial P}{\partial X}+\frac{\mu_{nf}}{\rho_{nf}\alpha_f}\left(\frac{\partial^2 U}{\partial X^2}+\frac{\partial^2 U}{\partial Y^2}\right)+\frac{(\rho\beta)_{nf}}{\rho_{nf}\beta_f}\mathrm{RaPr}\theta\sin(\Phi) \tag{2}$$

$$U\frac{\partial V}{\partial X}+V\frac{\partial V}{\partial Y}=-\frac{\partial P}{\partial Y}+\frac{\mu_{nf}}{\rho_{nf}\alpha_f}\left(\frac{\partial^2 V}{\partial X^2}+\frac{\partial^2 V}{\partial Y^2}\right)+\frac{(\rho\beta)_{nf}}{\rho_{nf}\beta_f}\mathrm{RaPr}\theta\cos(\Phi) \tag{3}$$

$$U\frac{\partial\theta}{\partial X}+V\frac{\partial\theta}{\partial Y}=\frac{\alpha_{nf}}{\alpha_f}\left(\frac{\partial^2\theta}{\partial X^2}+\frac{\partial^2\theta}{\partial Y^2}\right) \tag{4}$$

The effective density (ρ_{nf}), thermal expansion coefficient $(\beta)_{nf}$, heat capacitance $(C_p)_{nf}$ and thermal diffusivity (α_{nf}) of the nanofluid can be defined respectively as

$$\rho_{nf}=(1-\varphi)\rho_f+\varphi\rho_p$$

$$(\rho\beta)_{nf}=(1-\varphi)(\rho\beta)_f+\varphi(\rho\beta)_p$$

$$(\rho C_p)_{nf}=(1-\varphi)(\rho C_p)_f+\varphi(\rho C_p)_p$$

$$\alpha_{nf}=\frac{k_{nf}}{(\rho C_P)_{nf}}$$

The viscosity of the nanofluid is defined according to the Brinkman model and considered as a function of the solid volume fraction as given by Hwang et al. [40]:

$$\mu_{nf}=\frac{\mu_f}{(1-\varphi)^{2.5}}$$

while, the Maxwell correlation of the thermal conductivity of the nanofluid is considered in the present work as given by Hussein et al. [41].

$$k_{nf}=k_f\frac{(k_p+2k_f)-2\varphi(k_f-k_p)}{(k_p+2k_f)+\varphi(k_f-k_p)}$$

The flow field inside the wavy cavities can be represented by the stream function which is defined as follows:

$$U=\frac{\partial\psi}{\partial Y},\quad V=-\frac{\partial\psi}{\partial X}$$

This gives the following dimensionless equation:

$$\frac{\partial^2\psi}{\partial X^2}+\frac{\partial^2\psi}{\partial Y^2}=\frac{\partial U}{\partial Y}-\frac{\partial V}{\partial X} \tag{5}$$

The local and average Nusselt numbers are given by

$$\mathrm{Nu}=\frac{1}{\theta|_{\text{heat source wall}}}$$

The average Nusselt number ($\overline{\mathrm{Nu}}$) is determined by integration local Nusselt number along the heat source.

$$\overline{\mathrm{Nu}}=\frac{\int_{\text{along heat source}}\mathrm{Nu}\,dy}{\int_{\text{along heat source}}dy} \tag{6}$$

The heat flow inside the wavy cavities is represented by using the heat function (Π) concept as given by Basak et al. [42]:

$$\frac{\partial\Pi}{\partial Y}=U\theta-\frac{\alpha_{nf}}{\alpha_f}\frac{\partial\theta}{\partial X},\quad -\frac{\partial\Pi}{\partial X}=V\theta-\frac{\alpha_{nf}}{\alpha_f}\frac{\partial\theta}{\partial Y} \tag{7}$$

Or, it can be written in a single equation as follows:

$$\frac{\partial^2\Pi}{\partial X^2}+\frac{\partial^2\Pi}{\partial Y^2}=\frac{\partial}{\partial Y}(U\theta)-\frac{\partial}{\partial X}(V\theta) \tag{8}$$

The dimensionless boundary conditions of the present problem can be defined as

$$U(X,Y)=V(X,Y)=0,\theta=0,\psi=0,n\cdot\nabla\Pi=0$$
$$\text{For } X=0 \quad \text{and} \quad 0\leqslant Y\leqslant 0.5(1-\varepsilon)$$
$$U(0,Y)=V(0,Y)=0,\quad \frac{\partial\theta}{\partial X}=0=0,\quad \psi=0,\quad \Pi=0$$
$$\text{For } X=0 \quad \text{and} \quad 0.5(1-\varepsilon)\leqslant Y\leqslant 0.5(1+\varepsilon)$$
$$U(0,Y)=V(0,Y)=0,\frac{\partial\theta}{\partial X}=-\frac{k_f}{k_{nf}},\psi=0,\frac{\partial\Pi}{\partial X}=\frac{\alpha_{nf}}{\alpha_f}\frac{\partial\theta}{\partial Y}$$
$$\text{For } X=0 \quad \text{and} \quad 0.5(1-\varepsilon)\leqslant Y\leqslant 1$$
$$U(0,Y)=V(0,Y)=0,\frac{\partial\theta}{\partial X}=0=0,\psi=0,\Pi=0$$
$$\text{For } X=1 \quad \text{and} \quad 0\leqslant Y\leqslant 1$$
$$U(1,Y)=V(1,Y)=0,\frac{\partial\theta}{\partial X}=0,\psi=0,\Pi=\int_0^1\frac{\alpha_{nf}}{\alpha_f}\frac{\partial\theta}{\partial n}dY$$

The upper and lower walls of the cavities can be defined as

$$Y=\gamma\times\sin(2\pi N\times X) \text{ and } 0\leqslant X\leqslant 1$$

3. Numerical method of solution, verification and grid independent test

The non-linear behavior of the dimensionless mass, momentum and energy equations (Eqs. (1–4)) makes the analytical solution of these equations very complex to achieve. To avoid this problem, the finite volume method is used efficiently to solve these governing equations together with their dimensionless boundary conditions. The main object of the finite volume method is to convert the non-linear set of partial differential governing equations to a linear set of algebraic equations. The computational approach to solve the present problem starts by dividing the flow fields into various finite volumes and then solves the governing equations together with grid equations. More details about the method of solution can be found in [43]. To increase the accuracy of the numerical solution, additional grids are clustered adjacent to the wavy walls and near the discrete heat source in the left sidewall. The numerical solution continues by iteration until the convergence is satisfied. The cycle of numerical iteration stops when the maximum of residues of momentum and energy equations reaches less than or equal to 10^{-8}. Now, in order to check the accuracy of the present numerical results which are computed by our Fortran program, a comparison between the calculated average Nusselt number at the base together with temperature distribution and stream function in the present work with their corresponding results produced by Aminossadati and Ghasemi [39] for Cu–water nanofluid at $\varphi = 0.1$, $\varepsilon = 0.4$ and [Ra = 10^3–10^6] is performed and the final results of comparison are explained in Table 2. A good matching between the predicted results produced by the present program and the results of Aminossadati and Ghasemi [39] can be observed which gives a very good confirmation of the accuracy of our Fortran program. The present code is further validated against the existing numerical results of Adjlout el al., [19] for a wavy cavity flow at $Ra = 10^5$ as shown in Fig. 2. The results shown in Fig. 2 provide sufficient confidence for the present code. Another important step which is considered very necessary to ensure that there is no numerical divergence occurs in the computed results due to the gird sizing. So, grid independent tests are performed also. Table 3 shows these tests for verification of the flow and thermal fields in the case of the wavy cavity (Type I) filled with Ag–water nanofluid at $\varphi = 0.2$, $\varepsilon = 0.2$, $\gamma = 0.2$, $N = 1$ and Ra = 10^7. Ten groups of uniform gird sizes in X and Y directions are selected in these tests which are 30×30, 40×40, 50×50, 60×60, 70×70, 80×80, 90×90, 100×100, 120×120 and 140×140 respectively. Table 3 explains that the grid independence is achieved at the grid size of 100×100 where there is no deviation occurs in the flow and thermal fields after this grid size. Therefore, this grid size has been selected for the present numerical computations.

Table 2 Comparison between the calculated average Nusselt number at the base, temperature distribution and stream function in the present work with benchmark values of [39] for Cu–water nanofluid at $\varphi = 0.1$ & $\varepsilon = 0.4$ and [Ra = 10^3–10^6].

Ra	$\overline{Nu}_b$		θ_{max}		ψ_{max}	
	[39]	Present	[39]	Present	[39]	Present
10^3	5.45	5.44	0.205	0.203	0.023	0.022
10^4	5.47	5.51	0.205	0.204	0.251	0.249
10^5	7.12	7.14	0.172	0.171	2.988	2.986

4. Results and discussion

4.1. Effect of heating element length to cavity height ratio [ε] on flow and thermal fields

Fig. 3 illustrates streamline contours for three types of horizontal wavy cavity [$\Phi = 0°$] filled with Ag–water nanofluid at different values of the heating element length to the cavity height ratio [$\varepsilon = 0.2$, 0.4, 0.6, 0.8 and 1.0] and $N = 1$, $\gamma = 0.2$ with $\varphi = 0$ (dashed red line) and 0.2 (solid blue line) at Ra = 10^7. The flow field inside the cavities starts from the left sidewall due to the discrete heat source embedded in this region and moves upward due to the buoyancy force effect. The natural convection currents arrive firstly to the cold wavy upper wall and change their direction toward the adiabatic right sidewall. After that, they move toward the cold wavy bottom wall and return again to the hot region in the left sidewall. This cyclic rotation of the natural convection currents is the main reason for the flow vortices construction inside all types of wavy cavities. In fact, the purpose of Fig. 3 is to explain the effect of the heating element length to the cavity height ratio [ε] on the flow field inside the wavy cavities. It can be seen from the results of Fig. 3 (for type I) that as the [ε] increases from [$\varepsilon = 0.2$] to [$\varepsilon = 1.0$], the stream function increases from [$\psi_{max\ nf} = 0.28114$] to [$\psi_{max\ nf} = 3.0121$] for nanofluid (i.e., Ag–water). Also it increases from [$\psi_{max\ bf} = 4.3153$] to [$\psi_{max\ bf} = 10.216$] for base fluid (i.e., water). This is due to the increase in the area of the region exposed to a discrete isoflux heating in the left sidewall of the cavity as [ε] increases. This increase causes to enlarge the buoyancy force and natural convection currents and increases the intensity of the flow circulation inside the cavity. For type (II), the stream function increases as [ε] increases for nanofluid. With respect to the base fluid, it increases from [$\psi_{max\ bf} = 1.4462$] to [$\psi_{max\ bf} = 2.7944$] when [ε] increases from 0.2 to 0.4. But, it decreases from [$\psi_{max\ bf} = 2.4215$] at [$\varepsilon = 0.6$] to [$\psi_{max\ bf} = 1.8761$] at [$\varepsilon = 1.0$]. For

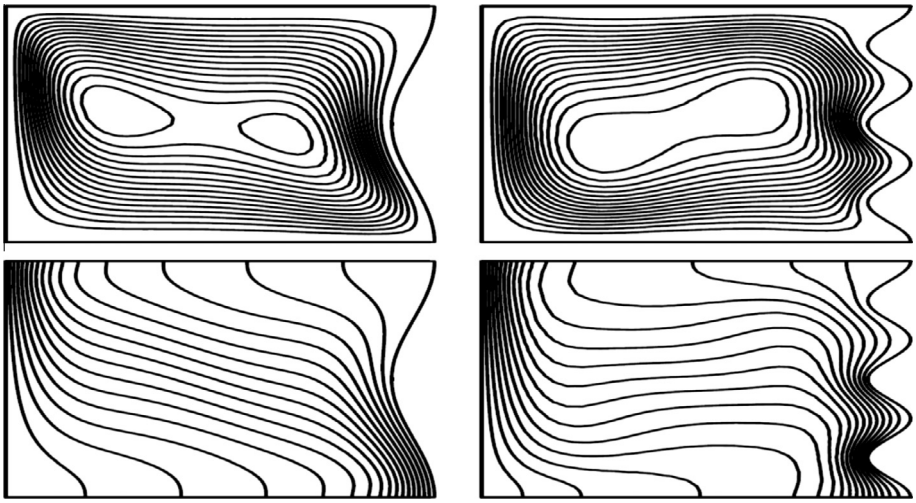

Figure 2 Streamfunction (Ψ) on the top and isotherms (θ) on the bottom, for a wavy cavity with cold left sidewall and hot right sidewall and adiabatic top and bottom walls at Ra = 10^5, Pr = 0.71 for $N = 1$, $\Phi = 60°$ on the left and $N = 3$, $\Phi = 90°$ on the right with the corresponding results of benchmark problem [19].

Table 3 Grid independence tests for verification in case of the wavy cavity (type I) filled Ag based nanofluid at $\varphi = \gamma = \varepsilon = 0.2$, $N = 1$ and Ra = 10^7.

Grid	$\lvert\psi_{max}\rvert$	θ_{max}	$\lvert\Pi_{max}\rvert$	$\overline{Nu}_s$
30 × 30	17.3373	0.07192	0.25371	58.3783
40 × 40	17.3197	0.06982	0.24387	57.8783
50 × 50	16.8207	0.06592	0.23463	56.2783
60 × 60	16.6107	0.06112	0.23137	55.9783
70 × 70	16.3055	0.05862	0.22944	54.6783
80 × 80	15. 9673	0.05268	0.21253	53.5883
90 × 90	15.80921	0.04482	0.20587	51.4483
100 × 100	15.7665	0.04193	0.19592	50.3783
120 × 120	15. 7665	0.04193	0.19592	50.3783
140 × 140	15. 7665	0.04193	0.19592	50.3783

type (III) the stream function decreases from [$\psi_{max\ nf} = -0.0968$] to [$\psi_{max\ nf} = -0.1351$] for nanofluid as [ε] increases from [$\varepsilon = 0.2$] to [$\varepsilon = 1.0$]. With respect to the base fluid, it increases as [ε] increases from 0.2 to 0.4. After that, it begins to decrease as [ε] increases from 0.6 to 1.0. Different modes of the flow field can be noticed for three types of wavy cavity. For type (I), it can be noticed that the flow field inside the cavity consists from rotating major convective vortices in the core of the cavity in addition to the two minor vortices adjacent to the upper and lower wavy walls. For type (II), the flow field consists from major vortices and one minor vortices near the lower wavy wall. For type (III), the minor vortices disappear in this geometry and as a result, the flow field consists from large major vortices. It is interesting to observe that the flow field for all three types becomes strong adjacent to the wavy walls. The thermal field inside the horizontal wavy cavities is represented by isotherm contours as explained in Fig. 4. The same parameters which are considered in Fig. 3 are used in this figure. First of all, it can be seen that isotherms are concentrated strongly adjacent to the left sidewall. This is due to the existence of the discrete isoflux heating at this wall. This phenomenon can be noticed for all three types of wavy cavities. Also, it can be seen that as [ε] increases from 0.2 to 1.0, the concentrated zone of isotherms increases due to the increase in the discrete isoflux heating region length as expected. For type (I), it can be noticed that the temperature distribution increases from [$\theta_{max\ nf} = 0.0581$] at [$\varepsilon = 0.2$] to [$\theta_{max\ nf} = 0.1197$] at [$\varepsilon = 1.0$] for nanofluid, while, it increases from [$\theta_{max\ bf} = 0.0429$] at [$\varepsilon = 0.2$] to [$\theta_{max\ bf} = 0.0828$] at [$\varepsilon = 1.0$] for base fluid. Similar increase in the temperature distributions for both base and nanofluids can be seen again for wavy cavities of types (II) and (III) respectively. The results of Fig. 4 show that the maximum temperature distribution for both base and nanofluids can be observed for the wavy cavity of type (I). Therefore, it can concluded from this result that the wavy cavity of type (I) can be considered as an optimum geometry for natural convection enhancement inside the wavy cavity. In fact, for the wavy cavity of type (I) it can be seen that the left sidewall [where the heat source exists] is shorter than the right sidewall. This of course makes the effect of the discrete isoflux heating or (ε) in this wall more pronounced and strong which leads to improve the flow and thermal fields in this type. With respect to the type (II), both left and right sidewalls have the same length, so the effect of the discrete isoflux heating or (ε) on the flow and thermal fields is moderate in this type. But, for the wavy cavity of type (III), the left sidewall [where the heat source exists] is longer than the right sidewall. This reduces the effect of the discrete isoflux heating or (ε) on the flow and thermal fields and causes a clear reduction in both the stream function and temperature distribution values for both base and nanofluids as shown in Figs. 3 and 4 respectively.

4.2. Effects of number of undulations and wave amplitude on flow and thermal fields

Fig. 5 explains streamline contours for three types of horizontal wavy cavity [$\Phi = 0°$] filled with Al_2O_3–water nanofluid at different values of N (number of undulations) and γ (wave amplitude) with $\varphi = 0$ (dashed red line) and 0.1 (solid blue line), $\varepsilon = 0.4$ and Ra = 10^6. With respect to the effect of

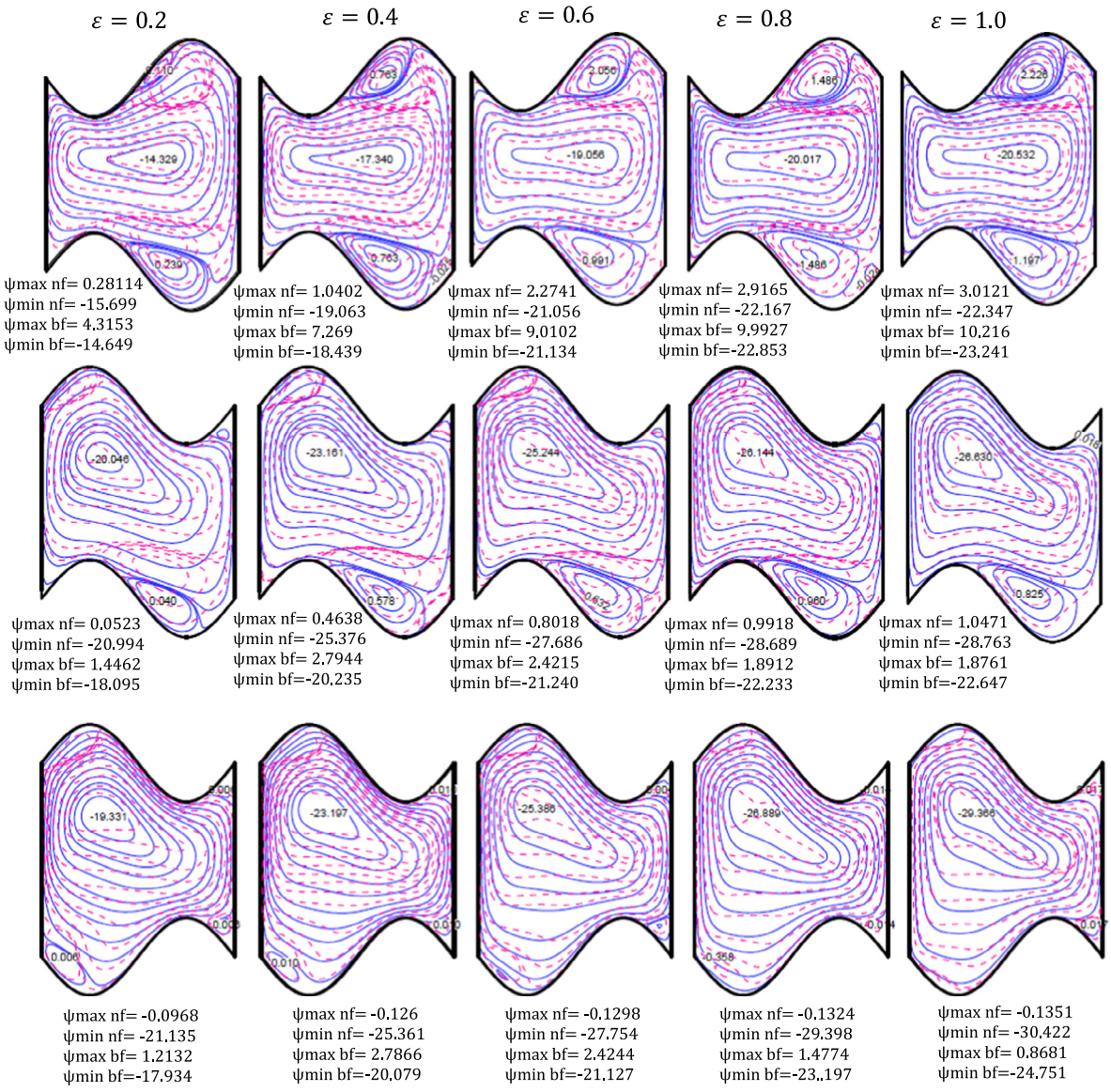

Figure 3 The contours of streamlines for three types of wavy cavity filled with Ag–water nanofluid at different values of $\varepsilon = 0.2, 0.4, 0.6, 0.8, 1$ for $N = 1$, $\gamma = 0.2$ & $\Phi = 0°$ with $\varphi = 0$ (dashed red line) & 0.2 (solid blue line) and $\mathrm{Ra} = 10^7$.

number of undulations on the flow field, it can be seen that for the horizontal wavy cavity of type (I), the stream function decreases for nanofluid from [$\psi_{\max\ nf} = 0.0135$] when [$N = 1$] to [$\psi_{\max\ nf} = -0.0381$] when [$N = 3$]. For base fluid, it increases from [$\psi_{\max\ bf} = -0.0705$] when [$N = 1$] to [$\psi_{\max\ bf} = -0.0181$] when [$N = 3$]. For type (II), it can be noticed that the stream function increases for nanofluid from [$\psi_{\max\ nf} = -0.0761$] when [$N = 1$] to [$\psi_{\max\ nf} = -0.0384$] when [$N = 3$]. For base fluid, it decreases from [$\psi_{\max\ bf} = -0.0164$] when [$N = 1$] to [$\psi_{\max\ bf} = -0.0189$] when [$N = 3$]. For type (III), it can be noticed that the stream function increases for nanofluid from [$\psi_{\max\ nf} = -0.0755$] when [$N = 1$] to [$\psi_{\max\ nf} = -0.0587$] when [$N = 3$]. For base fluid, it increases from [$\psi_{\max\ bf} = -0.0709$] when [$N = 1$] to [$\psi_{\max\ bf} = -0.0522$] when [$N = 3$]. Therefore, it can be concluded from results of Fig. 5, that the wavy cavity of type (I) with one undulation is the best option to increase the flow circulation of nanofluid, while, for base fluid the wavy cavity of type (II) with two undulations is the best option to increase the flow circulation. For this reason, wavy cavities of one and two undulations are better than the wavy cavity of three undulations. The reason of this behavior, is due to the increase in the flow separation for cavity with three undulations, which makes the flow to move in the reverse direction and decreases the stream function values. Furthermore, some minor vortices can be seen near the wavy walls especially when the wave amplitude is [$\gamma = 0.2$] and for three number of undulations. Fig. 6 shows isotherm contours for three types of horizontal wavy cavity [$\Phi = 0°$] filled with Al_2O_3–water nanofluid at different values of N (number of undulations) and γ (wave amplitude) with $\varphi = 0$ (dashed red line) and 0.1 (solid blue line), $\varepsilon = 0.4$ and $\mathrm{Ra} = 10^6$. It can be seen, that as the number of undulations increases from [$N = 1$] to [$N = 3$] for the horizontal wavy cavity of type (I), a slight decrease in the temperature distributions can be observed for both nano and base fluids, while a slight increase in the temperature distributions can be

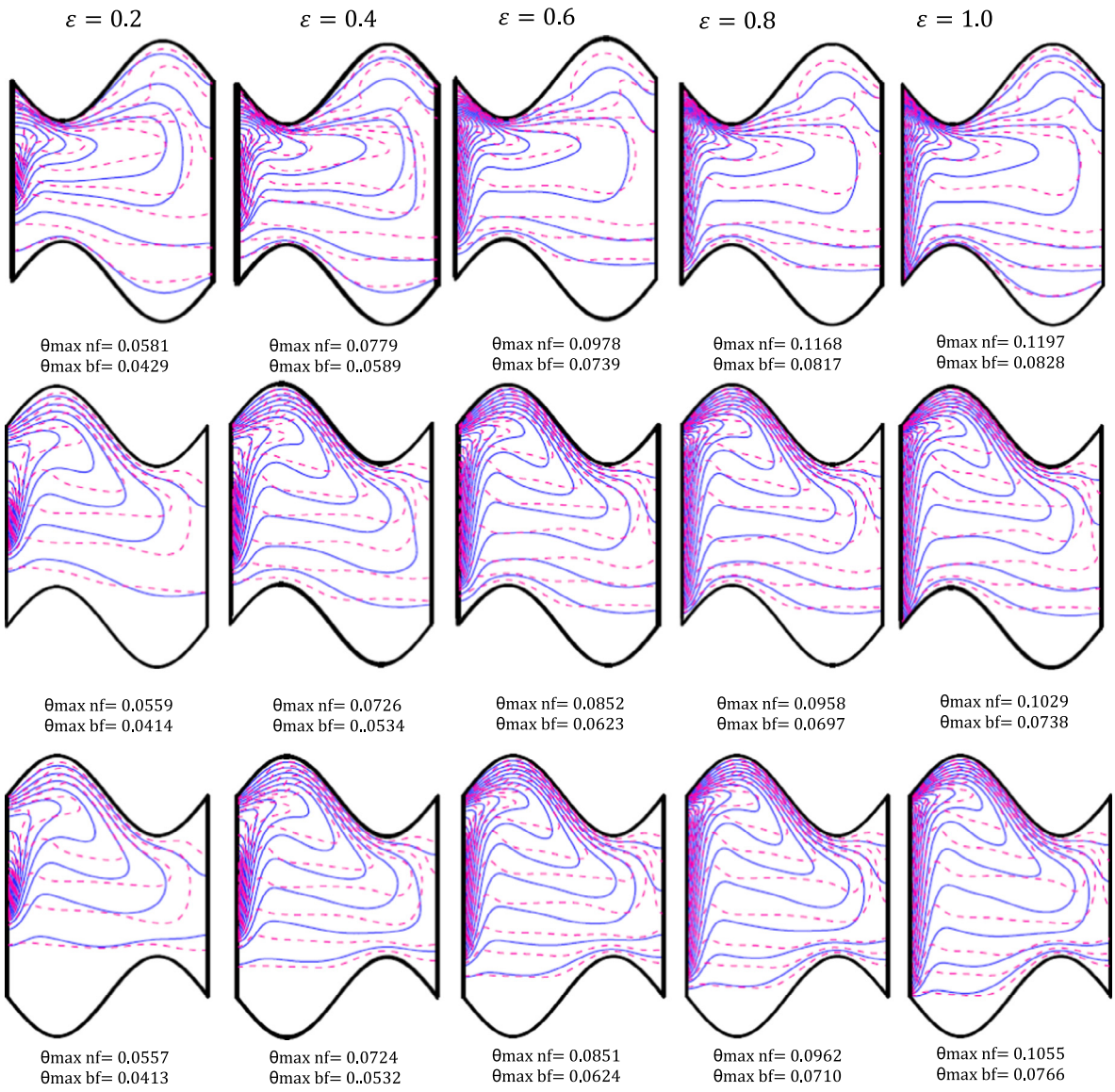

Figure 4 The contours of isotherms for three types of wavy cavity filled with Ag–water nanofluid at different values of $\varepsilon = 0.2, 0.4, 0.6, 0.8, 1$ for $N = 1$, $\gamma = 0.2$ & $\Phi = 0°$ with $\varphi = 0$ (dashed red line) & 0.2 (solid blue line) and $Ra = 10^7$.

seen for both nano and base fluids in wavy cavities of types (II) and (III) respectively. Anyway, the wavy cavity of type (I) with $[N = 1]$ is the best option to increase the thermal field for both nano and base fluids. With respect to the effect of the wave amplitude (γ) on the flow field, it can be seen that when the number of undulations is considered constant [i.e., $N = 3$] and as the wave amplitude increases from $[\gamma = 0.1]$ to $[\gamma = 0.2]$ for the horizontal wavy cavity of type (I), the stream function increases for nanofluid from $[\psi_{max\ nf} = -0.0381]$ to $[\psi_{max\ nf} = -0.0139]$, while, it increases for base fluid from $[\psi_{max\ bf} = -0.0181]$ to $[\psi_{max\ bf} = 0.0168]$. For types (II) and (III), similar increase in the stream function values can be seen for both nano and base fluids when the wave amplitude increases from $[\gamma = 0.1]$ to $[\gamma = 0.2]$. So, it can be deduced from results of Fig. 5, that the wavy cavity of type (II) with $[\gamma = 0.2]$ is the best option to increase the flow circulation for both nano and base fluids. Also, it can be observed from Fig. 5, that the streamlines coincide and take the geometry of the crest length or the inter-wall space of the wavy wall. On the other hand, the temperature distribution for all three types of horizontal wavy cavities increases slightly for both nano and base fluids when the wave amplitude increases from $[\gamma = 0.1]$ to $[\gamma = 0.2]$ as shown in Fig. 6. It can be seen that as the wave amplitude increases from $[\gamma = 0.1]$ to $[\gamma = 0.2]$, the crest length or the inter-wall space of the wavy wall increases and leads to increase the clustering of isotherms at this space. However, the wavy cavity of type (III) with $[\gamma = 0.2]$ is the best option to increase the thermal field for both nano and base fluids.

4.3. Effects of number of undulations and wave amplitude on heatlines contours

Fig. 7 illustrates contours of heatlines for three types of horizontal wavy cavity $[\Phi = 0°]$ filled with Al_2O_3–water nanofluid at different values of N (number of undulations) and γ (wave

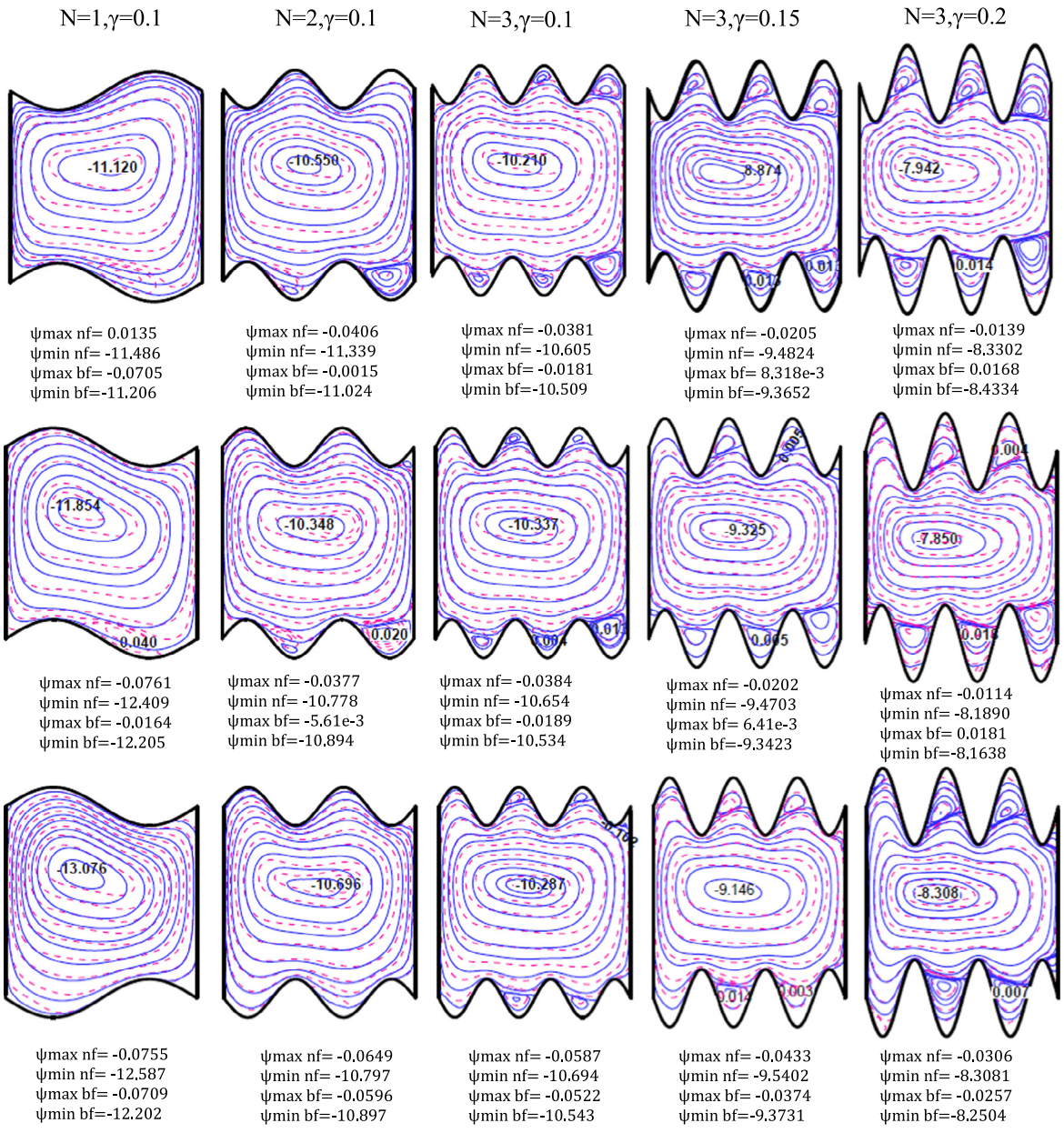

Figure 5 The contours of streamlines for three types of wavy cavity filled with Al_2O_3–water nanofluid at different values of N (number of undulations) and γ (wave amplitude) with $\varphi = 0$ (dashed red line) and 0.1 (solid blue line), $\Phi = 0°$, $\varepsilon = 0.4$ and $Ra = 10^6$.

amplitude) with $\varphi = 0$ (dashed red line) & 0.1 (solid blue line), $\varepsilon = 1$ and $Ra = 10^7$. In fact, heatlines technique gives a better overview about the heat transfer transport inside the wavy cavity, if they compared with the classical representation of heat flow via isotherms. The isotherms give an overview about the temperature distributions inside the cavities only, while, heatlines give a good picture about the heat transfer intensity and direction. With respect to the effect of number of undulations on the heat function (Π), it can be observed that for the horizontal wavy cavity of type (I), the heat function increases for nanofluid from [$\Pi_{max\ nf} = 0.6777$] when [$N = 1$] to [$\Pi_{max\ nf} = 0.7324$] when [$N = 3$]. For base fluid, it increases from [$\Pi_{max\ bf} = 0.6668$] when [$N = 1$] to [$\Pi_{max\ bf} = 0.7301$] when [$N = 3$]. For type (II), it can be seen that the heat function increases for nanofluid from [$\Pi_{max\ nf} = 0.7319$] when [$N = 1$] to [$\Pi_{max\ nf} = 0.8814$] when [$N = 3$]. For base fluid, it increases also from [$\Pi_{max\ bf} = 0.7302$] when [$N = 1$] to [$\Pi_{max\ bf} = 0.8793$] when [$N = 3$]. For type (III), it can be seen that the heat function decreases for nanofluid from [$\Pi_{max\ nf} = 0.7945$] when [$N = 1$] to [$\Pi_{max\ nf} = 0.7811$] when [$N = 3$]. For base fluid, it decreases also from [$\Pi_{max\ bf} = 0.7892$] when [$N = 1$] to [$\Pi_{max\ bf} = 0.7792$] when [$N = 3$]. So, it can be deduced from results of Fig. 7, that when the number of undulations increases from [$N = 1$] to [$N = 3$], heat functions increase for both nano and base fluids for wavy cavities of types (I) and (II) respectively, while, for wavy cavity of type (III), they decrease for both nano and base fluids when the number of undulations increases from [$N = 1$] to [$N = 3$]. In other words, the increase in the number of undulations causes an increase in the heat transfer inside wavy cavities of types (I) and (II), while the heat transfer amount decreases for wavy cavity of type (III) with the increase in the number of

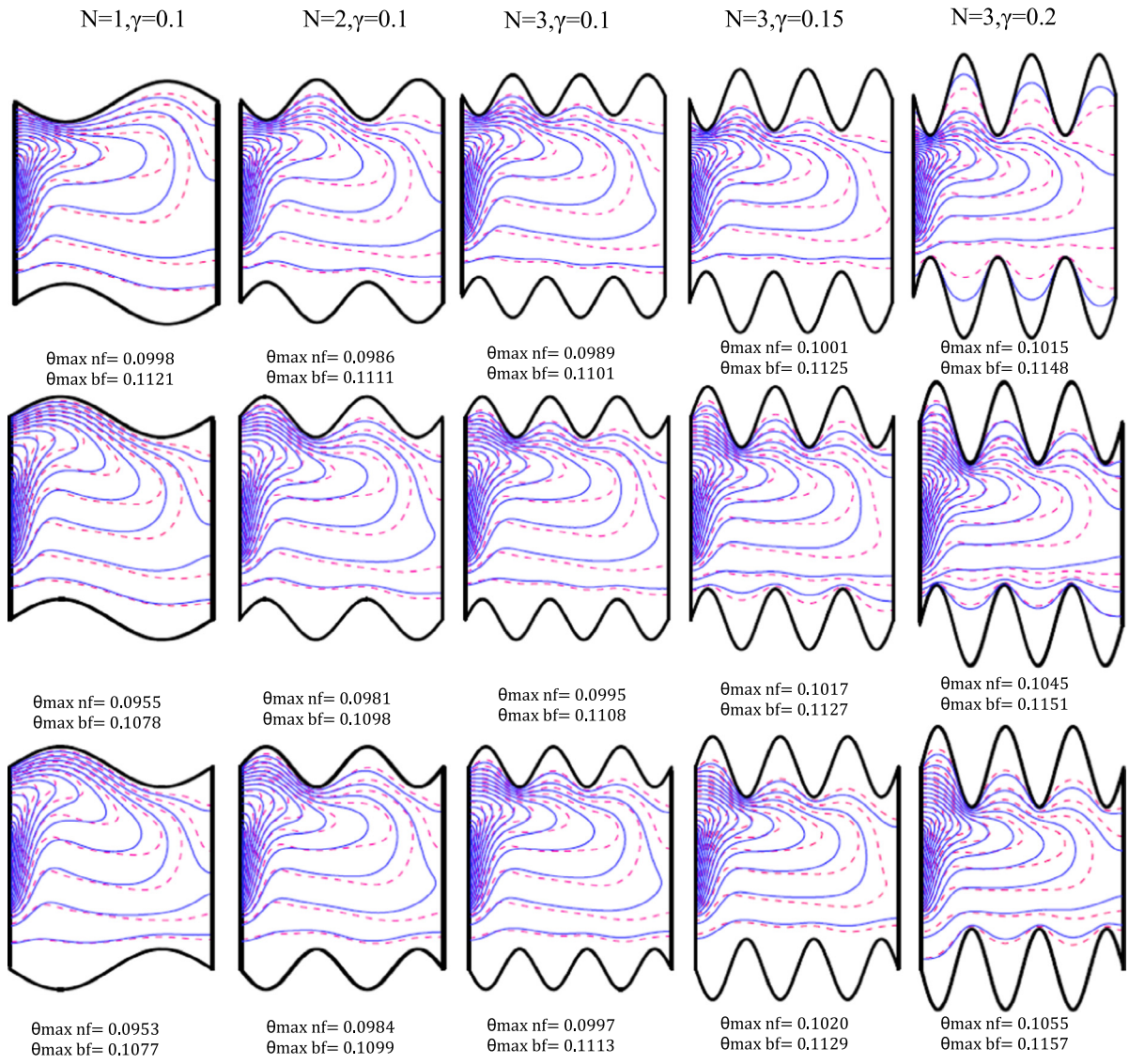

Figure 6 The contours of isotherms for three types of wavy cavity filled with Al_2O_3–water nanofluid at different values of N (number of undulations) and γ (wave amplitude) with $\varphi = 0$ (dashed red line) and 0.1 (solid blue line), $\Phi = 0°$, $\varepsilon = 0.4$ and $Ra = 10^6$.

undulations. With respect to the wave amplitude (γ) effect on the heat function (Π), it can be seen that for constant number of undulations [i.e., $N = 3$] and as the wave amplitude increases from [$\gamma = 0.1$] to [$\gamma = 0.2$] for the horizontal wavy cavity of type (I), the heat function increases for nanofluid from [$\Pi_{max\ nf} = 0.7324$] to [$\Pi_{max\ nf} = 0.8717$], while, it increases for base fluid from [$\Pi_{max\ bf} = 0.7301$] to [$\Pi_{max\ bf} = 0.8711$]. Similar increase in heat function values can be seen for types (II) and (III) respectively for both nano and base fluids when the wave amplitude increases from [$\gamma = 0.1$] to [$\gamma = 0.2$]. Therefore, in order to increase the heat function values or the heat transfer amount inside wavy cavities, one can do this by making an increase in the wave amplitude.

4.4. Effects of cavity inclination angle and Rayleigh number on flow and thermal fields

Fig. 8 displays streamline contours for the wavy cavity of type I as a case study filled with Al_2O_3–water nanofluid at different values of cavity inclination angle and Rayleigh number at [$\gamma = 0.1$, $\varepsilon = 0.2$] with $\varphi = 0$ (dashed red line) and 0.15 (solid blue line). For the horizontal wavy cavity [i.e., $\Phi = 0°$], it can be noticed that as the Rayleigh number increases from [$Ra = 10^4$] to [$Ra = 10^7$], a strong increase occurs in the stream function values for both nano and base fluids. For example, they increase for nanofluid from [$\psi_{max\ nf} = -1.74e{-}3$] at [$Ra = 10^4$] to [$\psi_{max\ nf} = 0.2763$] at [$Ra = 10^7$]. For base fluid, they increase also from [$\psi_{max\ bf} = -4.51e{-}3$] at [$Ra = 10^4$] to [$\psi_{max\ bf} = 1.2484$] at [$Ra = 10^7$]. This phenomenon is expected previously, since as the Rayleigh number increases, the buoyancy force and natural convection currents increase strongly. Therefore, the flow circulation velocity increases and leads as a result to increase the stream function values for both nano and base fluids. Also, a clear change occurs in the flow field patterns by converting it from symmetrical rotating vortices when the Rayleigh number is low [$Ra = 10^4$] to unsymmetrical major and minor vortices when the Rayleigh number is high [$Ra = 10^7$]. For inclined and

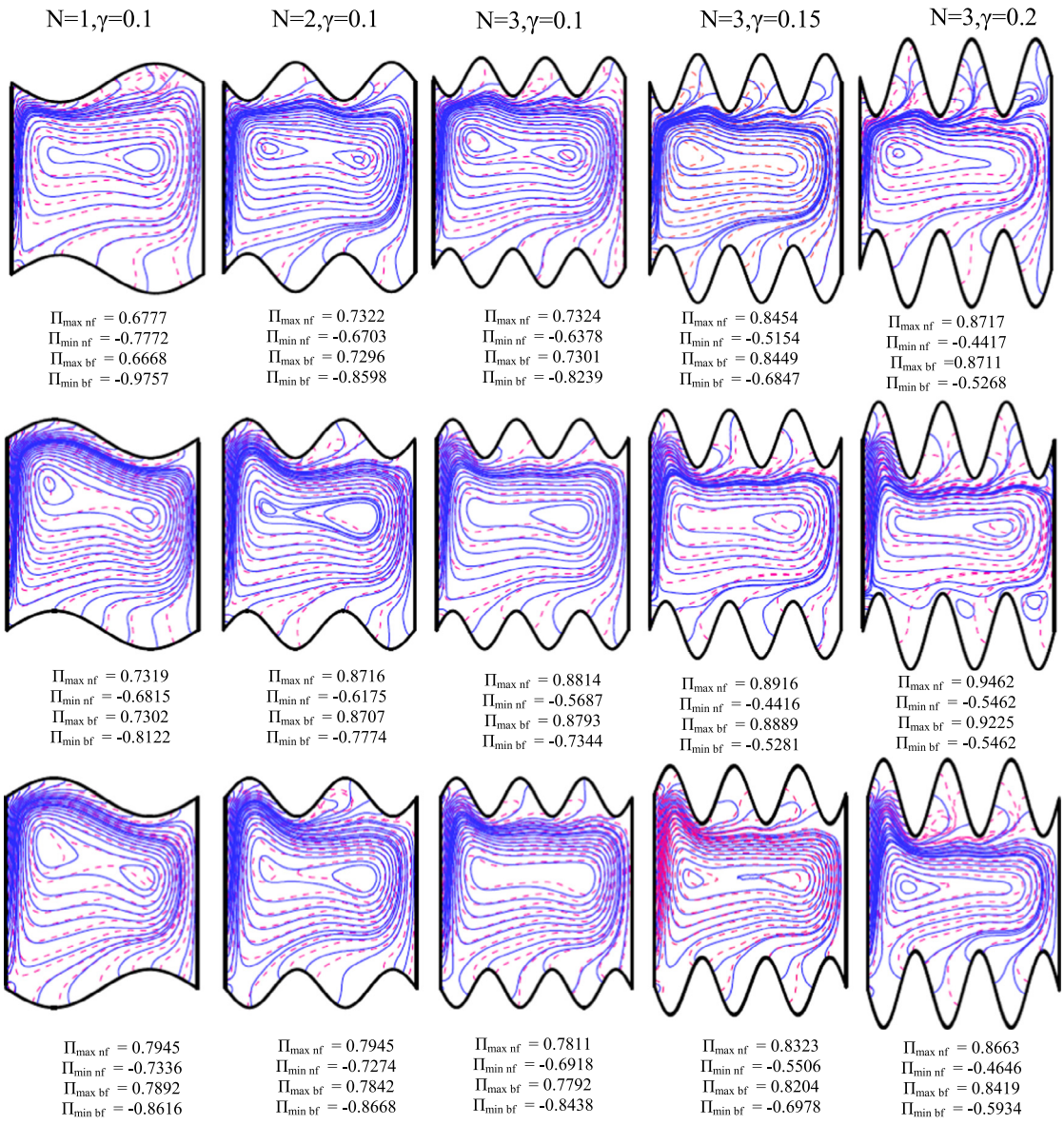

Figure 7 The contours of heatlines for three types of wavy cavity filled with Al_2O_3–water nanofluid at different values of N (number of undulations) and γ (wave amplitude) with $\varphi = 0$ (dashed red line) and 0.1 (solid blue line), $\Phi = 0°$, $\varepsilon = 1$ and $Ra = 10^7$.

vertical cavities, Fig. 8 shows that as the cavity inclination angle increases from [$\Phi = 30°$] to [$\Phi = 90°$], the stream function increases from [$\psi_{max\ nf} = -1.26e{-}3$] to [$\psi_{max\ nf} = 0.0518$] for nanofluid. Also, it increases from [$\psi_{max\ bf} = -3.35e{-}3$] to [$\psi_{max\ bf} = 0.1481$] for the base fluid. Also, the flow field changes from uniform rotating vortices at [$\Phi = 30°$] to symmetrical two rotating vortices at [$\Phi = 90°$]. Some minor vortices can be detected also at [$\Phi = 45°$ and $60°$] respectively. All these results are observed when the Rayleigh number is low [$Ra = 10^4$]. At high Rayleigh number [$Ra = 10^7$], a clear jump in the stream function values can be seen as the cavity inclination angle increases from [$\Phi = 30°$] to [$\Phi = 90°$]. For nano fluid, it increases from [$\psi_{max\ nf} = 5.2879$] at [$\Phi = 30°$] to [$\psi_{max\ nf} = 18.167$] at [$\Phi = 90°$], while, it increases also from [$\psi_{max\ bf} = 9.9822$] at [$\Phi = 30°$] to [$\psi_{max\ bf} = 21.581$] at [$\Phi = 90°$] for the base fluid. Also, a clear change occurs in the behavior of the flow patterns as the inclination angle increases from [$\Phi = 30°$] to [$\Phi = 90°$] and this variation becomes highly when [$Ra = 10^7$] due to the strong increase in the natural convection effect as explained previously. Therefore, the inclination angle plays an important role to increase the flow circulation inside the wavy cavity. Fig. 9 explains isotherm contours for the wavy cavity of type I filled with Al_2O_3–water nanofluid at different values of cavity inclination angle and Rayleigh number at $\varepsilon = 0.2$, $\gamma = 0.1$ with $\varphi = 0$ (dashed red line) and 0.15 (solid blue line). For the horizontal wavy cavity [i.e., $\Phi = 0°$], it can be noticed that a strong deformation occurs in the isotherms for both nano and base fluids as the Rayleigh number increases from [$Ra = 10^4$] to [$Ra = 10^7$]. This is due to the strong natural convection at [$Ra = 10^7$]. Also, when the Rayleigh number is low [$Ra = 10^4$], isotherms are emitted uniformly from the heat source at the left sidewall and distributed in a convenient pattern inside the cavity. This is because the conduction heat

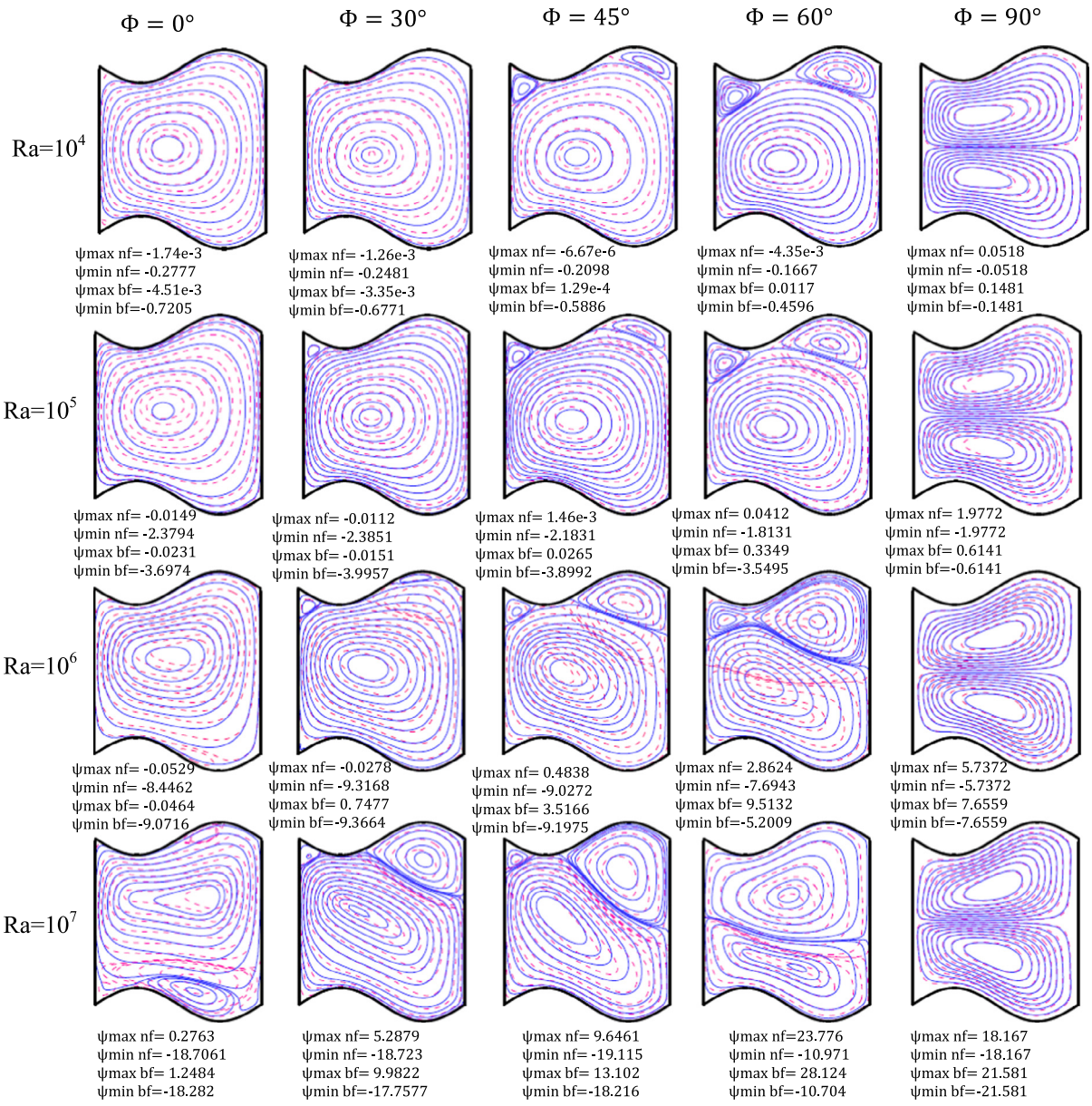

Figure 8 The contours of streamlines for the wavy cavity of type I filled with Al_2O_3–water nanofluid at different values of enclosure inclination angle and Rayleigh number at $\gamma = 0.1$, $\varepsilon = 0.2$ with $\varphi = 0$ (dashed red line) and 0.15 (solid blue line).

transfer is dominant at low Rayleigh number. On the other hand, a clear irregularity occurs in isotherms pattern at high Rayleigh number [Ra = 10^7]. Also, an intense clustering of isotherms is seen adjacent to the discrete heat source and the convection heat transfer is dominant in this case. For inclined and vertical cavities, Fig. 9 explains that as the cavity inclination angle increases from [$\Phi = 30°$] to [$\Phi = 90°$], the temperature distribution increases slightly from [$\theta_{max\ nf} = 0.1071$] to [$\theta_{max\ nf} = 0.1072$] for nanofluid. Also, it increases from [$\theta_{max\ bf} = 0.1657$] to [$\theta_{max\ bf} = 0.1679$] for the base fluid. These results are computed when the Rayleigh number is low [Ra = 10^4]. But, for high Rayleigh number [Ra = 10^7], it increases for nanofluid from [$\theta_{max\ nf} = 0.0457$] at [$\Phi = 30°$] to [$\theta_{max\ nf} = 0.0521$] at [$\Phi = 90°$], while, it increases from [$\theta_{max\ bf} = 0.0548$] at [$\Phi = 30°$] to [$\theta_{max\ bf} = 0.0629$] at [$\Phi = 90°$] for the base fluid. Again, the inclination angle and the Rayleigh number have a clear effect on patterns of isotherms as explained previously.

4.5. Effects of cavity inclination angle and Rayleigh number on heatlines contours

Fig. 10 illustrates contours of heatlines for the wavy cavity of type I filled with Al_2O_3–water nanofluid at different values of cavity inclination angle and Rayleigh number at $\varepsilon = 1$, $\gamma = 0.1$ with $\varphi = 0$ (dashed red line) and $\varphi = 0.15$ (solid blue line). The results explain that when the Rayleigh number increases from [Ra = 10^4] to [Ra = 10^6], the values of the heat function increase for nanofluid from [$\Pi_{max\ nf} = 0.7424$] to [$\Pi_{max\ nf} = 0.7554$], while, they increase for base fluid from [$\Pi_{max\ bf} = 0.7414$] to [$\Pi_{max\ bf} = 0.7431$]. This increase is due to the enhancement in the natural

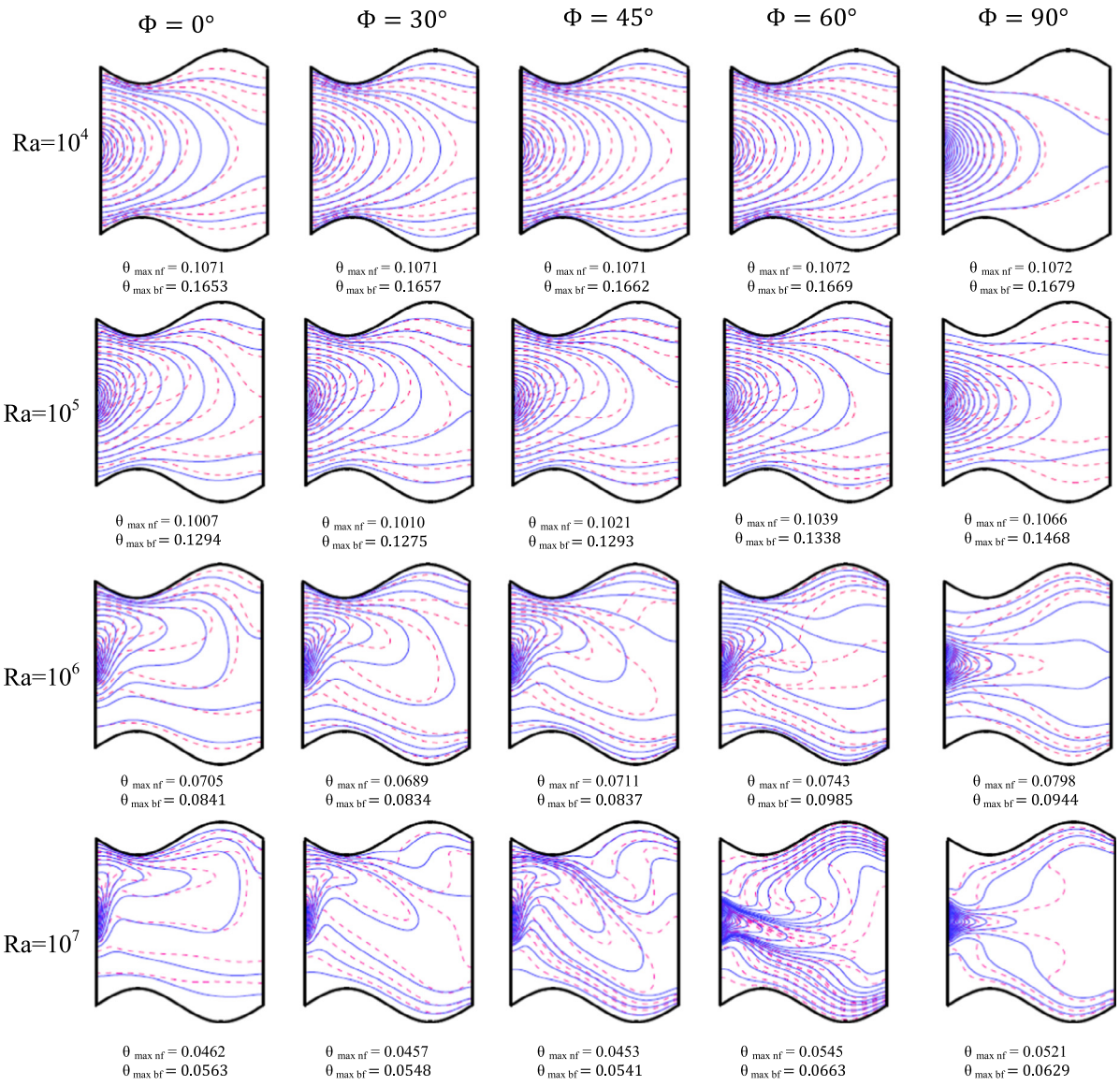

Figure 9 The contours of isotherms for the wavy cavity of type I filled with Al_2O_3–water nanofluid at different values of enclosure inclination angle and Rayleigh number at $\varepsilon = 0.2$, $\gamma = 0.1$ with $\varphi = 0$ (dashed red line) and 0.15 (solid blue line).

convection when the Rayleigh number increases from [Ra = 10^4] or conduction dominant case to [Ra = 10^6] or convection dominant case. When the wavy cavity is considered in an inclined position, the results of Fig. 10 show that at [Ra = 10^4] and when the inclination angle increases from [$\Phi = 30°$] to [$\Phi = 60°$], the heat function decreases from [$\Pi_{max\ nf} = 0.7431$] to [$\Pi_{max\ nf} = 0.7041$] for nanofluid. For base fluid, they decrease also from [$\Pi_{max\ bf} = 0.7413$] to [$\Pi_{max\ bf} = 0.7334$] for the same range of the inclination angle. Similar decrease in the heat function values for both nano and base fluids can be seen when the inclination angle increases from [$\Phi = 30°$] to [$\Phi = 60°$] at [Ra = 10^5] and [Ra = 10^6] respectively. On the other hand, when the cavity is converted from the horizontal position [$\Phi = 0°$] to the vertical one [$\Phi = 90°$], a clear decrease in heat function values can be seen for both nano and base fluids. This decrease can be observed for [Ra = 10^3–10^6]. With respect to the contours of heatlines at [Ra = 10^7], the results of Fig. 10 show that the values of the heat function for both base and nanofluids begin to drop suddenly for [$\Phi = 0°$–$60°$]. A reverse behavior can be seen at [$\Phi = 90°$]. Furthermore, the heatlines give a clear representation of the heat transfer path from the left sidewall where the heat source exists to both cold upper and lower walls. Moreover, results of Fig. 10 illustrate that the shape of heatline contours was greatly affected by both the Rayleigh number and the cavity inclination angle.

4.6. Effects of heating element length to cavity height ratio [ε] and inclination angle on the velocity profiles

Fig. 11 shows vertical velocity profiles along the mid-section of the wavy cavity (type I) for various heat source lengths and for (Ag–water, Ra = 10^7, $\Phi = 0°$, $N = 1$, $\gamma = 0.2$ and $\varphi = 0.1$). It is clearly seen that velocity profiles have positive values near the left sidewall of the cavity [$X = 0$] and the values of the velocity reach their maximum value when [$\varepsilon = 1$]. After that, the velocities begin to decrease gradually as [ε] decreases until

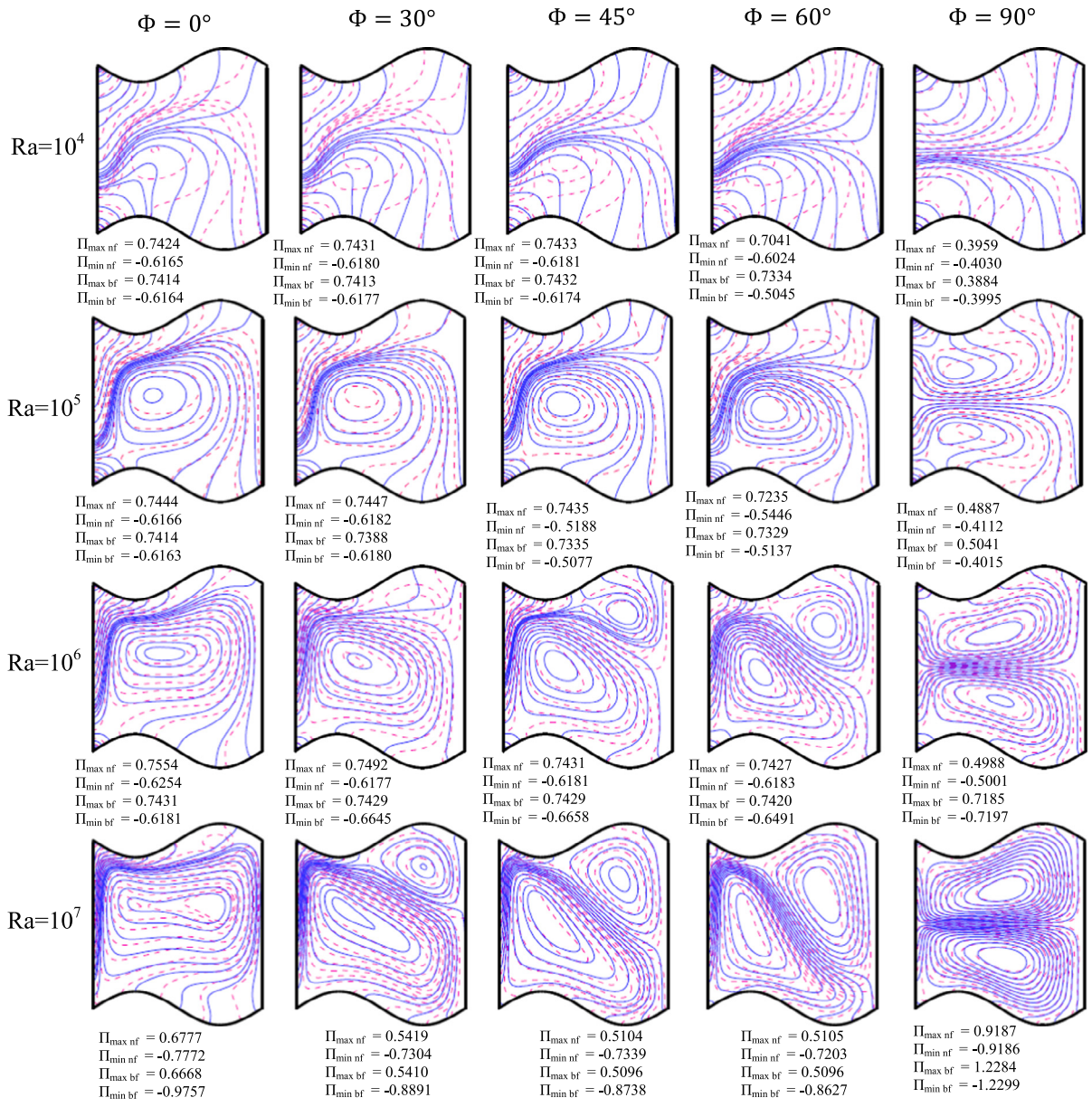

Figure 10 The contours of heatlines for the wavy cavity of type I filled with Al_2O_3–water nanofluid at different values of cavity inclination angle and Rayleigh number at $\varepsilon = 1$, $\gamma = 0.1$ with $\varphi = 0$ (dashed red line) & 0.15 (solid blue line).

they reach their minimum values at [$\varepsilon = 0.2$]. The reason of this increase in the velocity values at the left sidewall is due to the location of the heat source which causes a clear increase in the flow circulation. As the [ε] increases from [$\varepsilon = 0.2$] to [$\varepsilon = 1.0$], the heat source length increases and leads to increase the vertical velocity values. At [$X = 0.5$], the velocity profiles begin to fluctuate near their zero values. At [$X = 1.0$] or at the adiabatic right sidewall, a reverse behavior in the velocity profiles can be noticed while the velocities have negative values. Fig. 12 displays vertical velocity profiles along the mid-section of the wavy cavity of type I for various inclination angles and with Al_2O_3–water, $Ra = 10^7$, $\varepsilon = 0.2$, $N = 1$, $\gamma = 0.1$ and $\varphi = 0.05$. The results show that the velocity profiles have a linear variation and the vertical velocity values are zero at [$\Phi = 90°$]. In general, velocity profiles have minimum values at the middle of the cavity and this observation can be seen for various values of the inclination angles. This is due to the increase in the cross-sectional area of the considered cavity (i.e., type I). On the same manner, at the left sidewall [$X = 0$], the cross-sectional area is small, and as a result the velocity profiles have high values especially at [$\Phi = 45°$]. At the middle, they decrease due to the increase in the area as explained above. After that, the area of the wavy cavity (type I) begins to decrease again leading to increase the vertical velocity profiles until they reach zero value which satisfies the considered boundary conditions. Therefore, it can be concluded that the wavy geometry plays a significant role on the velocity profiles distribution.

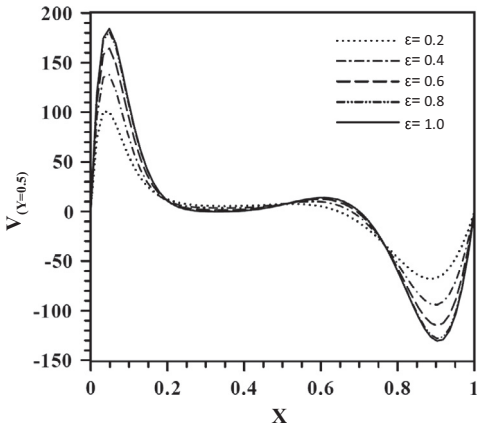

Figure 11 Vertical velocity profiles along the mid-section of the wavy cavity of type I for various heat source lengths (Ag–Water, Ra = 10^7, $\Phi = 0°$, $N = 1$, $\gamma = 0.2$ and $\varphi = 0.1$).

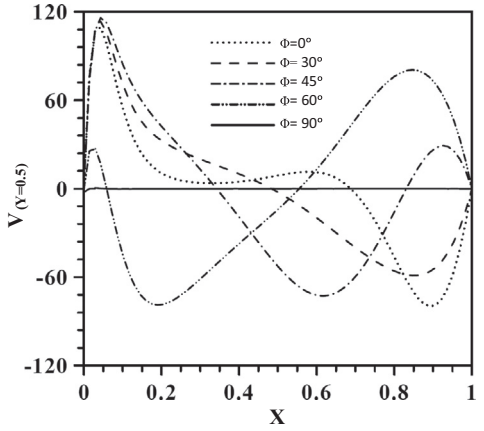

Figure 12 Vertical velocity profiles along the mid-section of the wavy cavity of type I for various inclination angles (Al_2O_3–Water, Ra = 10^7, $\varepsilon = 0.2$, $N = 1$, $\gamma = 0.1$ and $\varphi = 0.05$).

4.7. Effects of heating element length to cavity height ratio [ε] and inclination angle on the local Nusselt number

Fig. 13 shows the variation of the local Nusselt number of Ag–water nanofluid of a horizontal wavy cavity of type III along the heat source for various heating element length to cavity height ratio [ε] at Ra = 10^7, $\Phi = 0°$, $N = 1$, $\gamma = 0.2$ and $\varphi = 0.2$. It can be noticed from the results that as [ε] increases, the local Nusselt number along the heat source decreases. This behavior is because, when [ε] increases the heat source length increases. This causes to increase the area exposed to the convection heat transfer and leads to increase the heat dissipation along the heat source. As a result of the heat dissipation adjacent to the heat source, the temperature gradient begins to decrease gradually and leads to decrease the local Nusselt number. Fig. 14 illustrates the variation of the local Nusselt number of Al_2O_3–water nanofluid of a wavy cavity (type I) along the heat source for various inclination angles at Ra = 10^6, $\varepsilon = 0.2$, $N = 1$, $\gamma = 0.1$ and $\varphi = 0.1$. It can be seen that when the wavy cavity is inclined at $\Phi = 30°$ and 45°, the local Nusselt number along the heat source has

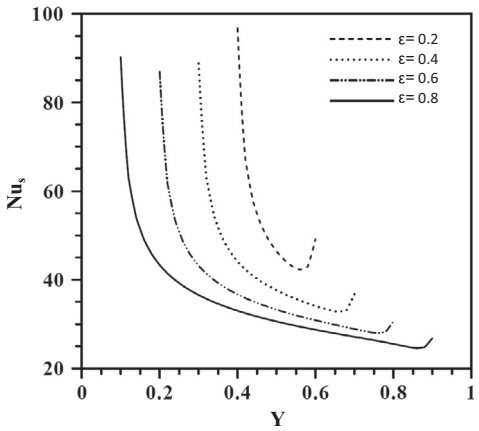

Figure 13 Variation of the local Nusselt number of a silver-based nanofluid of a wavy cavity (type:III) along the heat source for various heating element length to cavity height ratio at Ra = 10^7, $\Phi = 0°$, $N = 1$, $\gamma = 0.2$ and $\varphi = 0.2$.

a maximum value. After that, it begins to decrease gradually as the wavy cavity is converted from the horizontal position [$\Phi = 0°$] to the vertical position [$\Phi = 90°$]. This result ensures that, the local Nusselt number can be enhanced, when the wavy cavity is inclined at $\Phi = 30°$ and 45° respectively.

4.8. Effects of solid volume fraction and wave amplitude on the local Nusselt number

Fig. 15 illustrates the variation of the local Nusselt number of Al_2O_3–water nanofluid of a wavy cavity (type II) along the heat source for various solid volume fractions and wave amplitudes at Ra = 10^5, $\varepsilon = 0.4$, $N = 3$ and $\Phi = 0°$. It can be seen from the results of Fig. 15, that as the solid volume fractions and wave amplitudes increase, the local Nusselt number along the heat source increases. It can be seen that the maximum local Nusselt number occurs for maximum values of solid volume fraction and wave amplitudes [i.e. $\varphi = 0.2$ and $\gamma = 0.2$], while, the minimum local Nusselt number occurs for zero solid

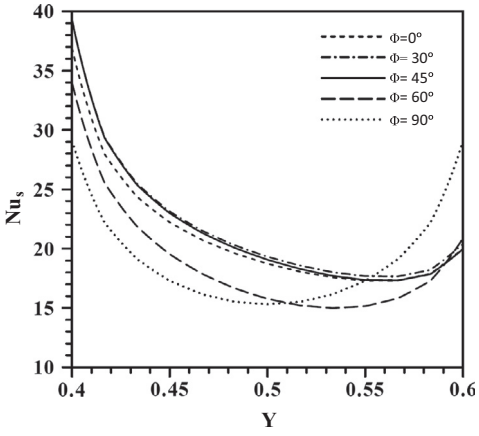

Figure 14 Variation of the local Nusselt number of an Alumina-based nanofluid of a wavy cavity (type:I) along the heat source for various inclination angles at Ra = 10^6, $\varepsilon = 0.2$, $N = 1$, $\gamma = 0.1$ and $\varphi = 0.1$.

volume fraction [$\varphi = 0$ or for base fluid only] and wave amplitudes [$\gamma = 0.1$]. Therefore, this result indicates that the addition of solid Al_2O_3 nano particles makes an important enhancement of the local Nusselt number. The reason of this behavior is due to the increase in the effective thermal conductivity of nanofluid with the increase in the solid volume fraction. The same enhancement can be satisfied by increasing the amplitude of the wavy wall.

4.9. Effects of nanofluid type and Rayleigh number on the average Nusselt number

Fig. 16 shows the variation of the average Nusselt number along the heat source with heating element length to cavity height ratio [ε] of Al_2O_3–water and Ag–water nanofluids in a wavy cavity (type II) for various Rayleigh numbers at $\gamma = 0.2$, $N = 1$, $\varphi = 0.1$ and $\Phi = 0°$. It can be noticed that the average Nusselt number increases for both types of nanofluid as the Rayleigh number increases. The reason of this phenomenon is due to the high effect of natural convection which leads to increase the average Nusselt number along the heat source. Moreover, it can be seen from the results, that the average Nusselt number with the addition of Ag nanoparticles is greater than the corresponding value with the addition of Al_2O_3 nanoparticles especially for Ra = 10^7. The reason of this phenomenon is due to the high difference between the thermal conductivities of Ag and Al_2O_3 nanoparticles as can be seen in Table 1.

4.10. Effect of inclination angle on the average Nusselt number

Fig. 17 displays the variation of the average Nusselt number along the heat source with inclination angles of Al_2O_3 and Ag based nanofluids in a wavy cavity (type I) for various Rayleigh numbers at $\gamma = 0.1$, $N = 1$, $\varphi = 0.1$ and $\varepsilon = 0.2$. It is seen that for high values of the Rayleigh number [i.e., Ra = 10^7], the average Nusselt number reaches its maximum

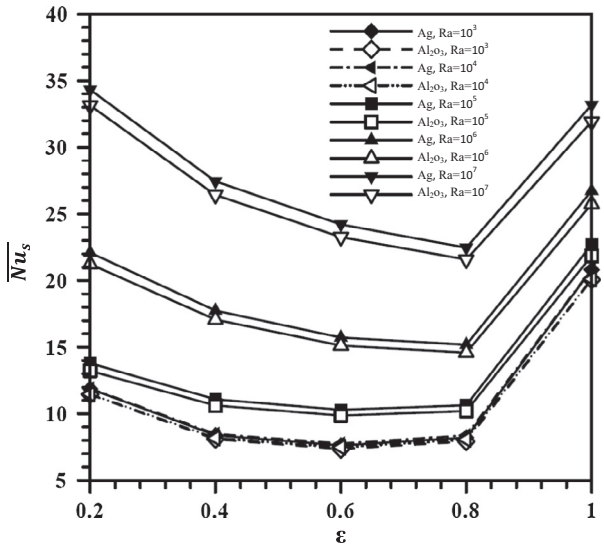

Figure 16 Variation of average Nusselt number along the heat source with heating element length to cavity height ratio [ε] of Al_2O_3–water and Ag–water nanofluids in a wavy cavity (type:II) for various Rayleigh numbers at $\gamma = 0.2$, $N = 1$, $\varphi = 0.1$ and $\Phi = 0°$.

value for both Al_2O_3–water and Ag–water nanofluids. This behavior is due to the increase in the convection heat transfer and flow circulation strength which leads to increase the thermal energy transport inside the cavity and causes to increase the average Nusselt number. It can be seen also from Fig. 17, that there is a linear variation of the average Nusselt number with the inclination angle when the Rayleigh number is low [Ra = 10^3 and 10^4]. This is due to the conduction effect which encountered at low values of Rayleigh number. So, it can be concluded that the inclination angle has a very weak effect on the average Nusselt number for low values of

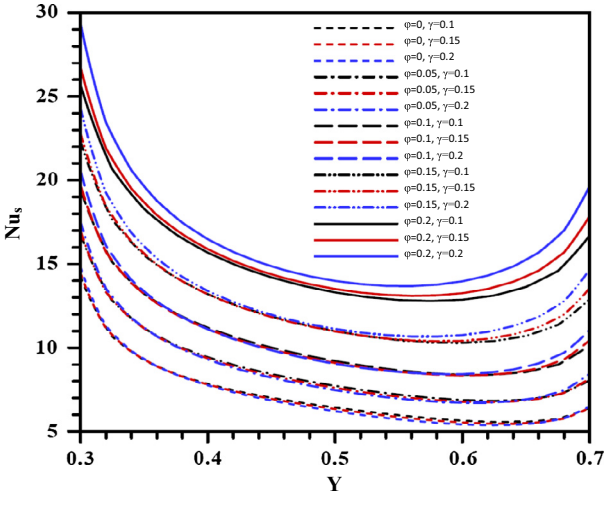

Figure 15 Variation of the local Nusselt number of Al_2O_3–water nanofluid of a wavy cavity (type:II) along the heat source for various volume fractions and wave amplitudes at Ra = 10^5, $\varepsilon = 0.4$, $N = 3$ and $\Phi = 0°$.

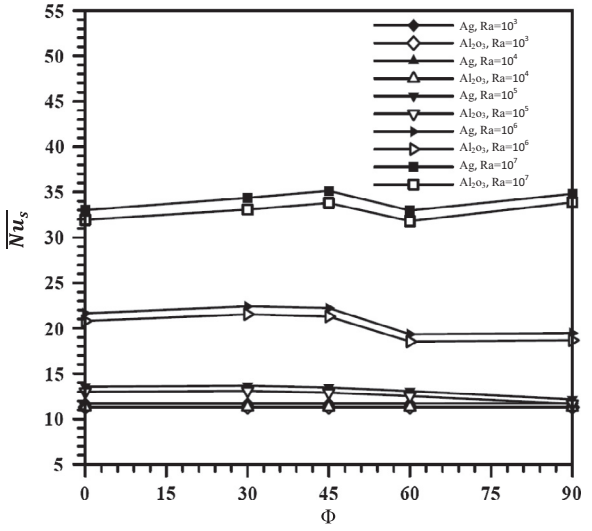

Figure 17 Variation of average Nusselt number along the heat source with inclination angles of Al_2O_3–water and Ag–water nanofluids in a wavy cavity (type:I) for various Rayleigh numbers at $\gamma = 0.1$, $N = 1$, $\varphi = 0.1$ and $\varepsilon = 0.2$.

Rayleigh number. Again, for [Ra = 10^6 and 10^7] the average Nusselt number with the addition of Ag nanoparticles is greater than its value with the addition of Al_2O_3 nanoparticles for the same reason explained previously.

5. Conclusions

Natural convection visualization by heatlines in three types of inclined wavy cavities filled with Al_2O_3–water and Ag–water nanofluids and subjected to a discrete isoflux heating from its left sidewall is investigated numerically in this work. It is found that for horizontal wavy cavity (type I), the stream functions for both base and nanofluids increase as [ε] increases from 0.2 to 1.0. The geometry of the wavy cavity has an important role on the flow and thermal fields where different patterns of these fields can be seen for three types of wavy cavity. Also, it is found that for all three types of horizontal wavy cavities, the concentrated zone of isotherms near the left sidewall increases as [ε] increases from 0.2 to 1.0 and the temperature distributions for both base and nanofluids increase. Moreover, the flow circulation of both nano and base fluids inside the cavity increases when the wave amplitude increases. The wavy cavity of type (II) with [$\gamma = 0.2$] is the best option to increase the flow circulation for both nano and base fluids, while, the horizontal wavy cavity of type (I) can be selected as an optimum geometry for natural convection enhancement for both base and nanofluids. On the other hand, the temperature distribution for all three types of horizontal wavy cavities increases slightly for both nano and base fluids when the wave amplitude increases. Type (III) with [$\gamma = 0.2$] is the best option to increase the thermal field for both nano and base fluids. From the computed results, it can be concluded that when the number of undulations increases, heat functions increase for both nano and base fluids for wavy cavities of types (I) and (II), while, for wavy cavity of type (III), they decrease for both nano and base fluids when the number of undulations increases. The local Nusselt number along the heat source decreases as [ε] increases, while it increases when the wavy cavity is inclined at [$\Phi = 30°$ and $45°$] respectively and when the solid volume fractions and wave amplitudes increase. For high Rayleigh number, the average Nusselt number with the addition of Ag nanoparticles is greater than the corresponding value with the addition of Al_2O_3 nanoparticles. The relationship between the inclination angle and the average Nusselt number is very weak for low values of Rayleigh number. This behavior can be seen for both (Al_2O_3) and (Ag) nanoparticles. Furthermore, the velocity profiles have positive values near the left sidewall of the cavity [$X = 0$] and increase as [ε] increases. At [$X = 0.5$], they fluctuate around zero values, while at the right sidewall of the cavity [$X = 1$] they have negative values and decrease as [ε] increases. While, it is found also that they have a linear variation at [$\Phi = 90°$] and a wavy behavior for another values of the inclination angles. Finally, the results of the present work illustrate that for all three types of horizontal wavy cavities, heat functions increase for both nano and base fluids when the wave amplitude and the Rayleigh number increase.

References

[1] C. RamReddy, P. Murthy, A. Chamkha, A. Rashad, Soret effect on mixed convection flow in a nanofluid under convective boundary condition, Int. J. Heat Mass Transf. 64 (2013) 384–392.

[2] E. Abu-Nada, A. Chamkha, Effect of nanofluid variable properties on natural convection in enclosures filled with an CuO–EG–water nanofluid, Int. J. Therm. Sci. 49 (2010) 2339–2352.

[3] E. Abu-Nada, A. Chamkha, Mixed convection flow in a lid-driven inclined square enclosure filled with a nanofluid, Eur. J. Mech. B. Fluids 29 (2010) 472–482.

[4] S. Parvin, R. Nasrin, M. Alim, N. Hossain, A. Chamkha, Thermal conductivity variation on natural convection flow of water–alumina nanofluid in an annulus, Int. J. Heat Mass Transf. 55 (2012) 5268–5274.

[5] A. Chamkha, A. Rashad, Natural convection from a vertical permeable cone in a nanofluid saturated porous media for uniform heat and nanoparticles volume fraction fluxes, Int. J. Numer. Methods Heat Fluid Flow 22 (2012) 1073–1085.

[6] R. Nasrin, M. Alim, A. Chamkha, Numerical simulation of non-Darcy forced convection through a channel with non-uniform heat flux in an open cavity using nanofluid, Numer. Heat Transfer – Part A 64 (2013) 820–840.

[7] M. Mansour, M. Bakier, A. Chamkha, Natural convection inside a C-shaped nanofluid-filled enclosure with localized heat sources, Int. J. Numer. Meth. Heat Fluid Flow 24 (2014) 1954–1978.

[8] S. Ahmed, A. Hussein, H. Mohammed, S. Sivasankaran, Boundary layer flow and heat transfer due to permeable stretching tube in the presence of heat source/sink utilizing nanofluids, Appl. Math. Comput. 238 (2014) 149–162.

[9] S. Murshed, K. Leong, C. Yang, Thermo-physical and electro-kinetic properties of nanofluids – a critical review, Appl. Therm. Eng. 28 (2008) 2109–2125.

[10] L. Wang, M. Quintard, Nanofluids of the future, Advances in Transport Phenomena 1 (2009) 179–243.

[11] R. Saidur, K. Leong, H. Mohammad, A review on applications and challenges of nanofluids, Renew. Sustain. Energy Rev. 15 (2011) 1646–1668.

[12] B. Calcagni, F. Marsili, M. Paroncini, Natural convective heat transfer in square enclosures heated from below, Appl. Therm. Eng. 25 (2005) 2522–2531.

[13] S. Hussain, A. Hussein, Natural convection heat transfer in a differentially heated square enclosure with a heat generating-conducting circular cylinder at different diagonal locations, in: 6th International Advanced Technologies Symposium Proceedings (IATS'11), Elazığ, Turkey, 16–18 May, 2011, pp. 13–19.

[14] L. Khezzar, D. Siginer, I. Vinogradov, Natural convection in inclined two dimensional rectangular cavities, Heat Mass Transf. 48 (2012) 227–239.

[15] L. Kolsi, A. Hussein, M. Borjini, H. Mohammed, H. Ben Aïssia, Computational analysis of three-dimensional unsteady natural convection and entropy generation in a cubical enclosure filled with water–Al_2O_3 nanofluid, Arab. J. Sci. Eng. 39 (2014) 7483–7493.

[16] Y. He, C. Qi, Y. Hu, B. Qin, F. Li, Y. Ding, Lattice Boltzmann simulation of alumina–water nanofluid in a square cavity, Nanoscale Res. Lett. 6 (2011) 184–191.

[17] G. Sheikhzadeh, A. Arefmanesh, M. Kheirkhah, R. Abdollahi, Natural convection of Cu–water nanofluid in a cavity with partially active sidewalls, Eur. J. Mech. B/Fluids 30 (2011) 166–176.

[18] S. Mahmud, P. Das, N. Hyder, A. Islam, Free convection heat transfer in an enclosure with vertical wavy walls, Int. J. Therm. Sci. 41 (2002) 440–446.
[19] L. Adjlout, O. Imine, A. Azzi, M. Belkadi, Laminar natural convection in an inclined cavity with a wavy wall, Int. J. Heat Mass Transf. 45 (2002) 2141–2152.
[20] P. Das, S. Mahmud, S. Tasnim, Sadrul. Islam, A. Effect of surface waviness and aspect ratio on heat transfer inside a wavy enclosure, Int. J. Numer. Meth. Heat Fluid Flow 13 (8) (2003) 1097–1122.
[21] K. Mushatet, Simulation of natural convection in an inclined square cavity with two wavy walls, J. Appl. Sci. Res. 6 (12) (2010) 2111–2122.
[22] A. Bendehina, O. Imine, L. Adjlout, Laminar free convection in undulated cavity with non-uniform boundary conditions, C.R. Mec. 339 (2011) 42–57.
[23] L. Adjlout, O. Imine, A. Azzi, M. Belkadi, Numerical study of the natural convection in a cavity with undulated wall, in: Third International Thermal Energy and Environment Congress, Marrakech, Morocco, June 9–12, 1997.
[24] S. Abdelkader, R. Mebrouk, B. Abdellah, B. Khadidja, Natural convection in a horizontal wavy enclosure, J. Appl. Sci. 7 (2007) 334–341.
[25] J. Rostami, Unsteady natural convection in an enclosure with vertical wavy walls, Heat Mass Transf. 44 (2008) 1079–1087.
[26] S. Hussain, A. Hussein, M. Mahdi, Natural convection in a square inclined enclosure with vee-corrugated sidewalls subjected to constant flux heating from below, Nonlinear Anal.: Modell. Control 16 (2) (2011) 152–169.
[27] H. Oztop, E. Abu-Nada, Y. Varol, A. Chamkha, Natural convection in wavy enclosures with volumetric heat sources, Int. J. Therm. Sci. 50 (2011) 502–514.
[28] C. Chang Cho, C. Li Chen, C. Kuang Chen, Natural convection heat transfer performance in complex-wavy-wall enclosed cavity filled with nanofluid, Int. J. Therm. Sci. 60 (2012) 255–263.
[29] M. Nikfar, M. Mahmoodi, Meshless local Petrov–Galerkin analysis of free convection of nanofluid in a cavity with wavy sidewalls, Eng. Anal. Boundary Elem. 36 (2012) 433–445.
[30] M. Esmaeilpour, M. Abdollahzadeh, Free convection and entropy generation of nanofluid inside an enclosure with different patterns of vertical wavy walls, Int. J. Therm. Sci. 52 (2012) 127–136.
[31] C. Chang Cho, H. Terng Yau, C. Kuang Chen, Numerical investigation into natural convection heat transfer enhancement of copper–water nanofluid in a wavy wall enclosure, Thermal Sci. 16 (5) (2012) 1309–1316.
[32] M. Mansour, M. Bakier, Free convection heat transfer in complex-wavy-wall enclosed cavity filled with nanofluid, Int. Commun. Heat Mass Transfer 44 (2013) 108–115.
[33] R. Nasrin, M. Alim, A. Chamkha, Combined convection flow in triangular wavy chamber filled with water–CuO nanofluid: effect of viscosity models, Int. Commun. Heat Mass Transfer 39 (2012) 1226–1236.
[34] E. Abu-Nada, A. Chamkha, Mixed convection flow of a nanofluid in a lid-driven cavity with a wavy wall, Int. Commun. Heat Mass Transfer 57 (2014) 36–47.
[35] S. Kimura, A. Bejan, The heatline visualization of convective heat transfer, ASME J. Heat Transfer 105 (1983) 916–919.
[36] V. Costa, Bejan's heatlines and masslines for convection visualization and analysis, Appl. Mech. Rev. 59 (2006) 126–145.
[37] H. Oztop, M. Mobedi, E. Abu-Nada, I. Pop, A heatline analysis of natural convection in a square inclined enclosure filled with a CuO nanofluid under non-uniform wall heating condition, Int. J. Heat Mass Transf. 55 (2012) 5076–5086.
[38] T. Basak, A. Chamkha, Heatline analysis on natural convection for nanofluids confined within square cavities with various thermal boundary conditions, Int. J. Heat Mass Transf. 55 (2012) 5526–5543.
[39] S. Aminossadati, B. Ghasemi, Natural convection cooling of a localised heat source at the bottom of a nanofluid-filled enclosure, Eur. J. Mech. B/Fluids 28 (2009) 630–640.
[40] K. Hwang, J. Lee, S. Jang, Buoyancy-driven heat transfer of water-based Al_2O_3 nanofluids in a rectangular cavity, Int. J. Heat Mass Transf. 50 (2007) 4003–4010.
[41] A. Hussein, H. Ashorynejad, M. Shikholeslami, S. Sivasankaran, Lattice Boltzmann simulation of natural convection heat transfer in an open enclosure filled with Cu–water nanofluid in a presence of magnetic field, Nucl. Eng. Des. 268 (2014) 10–17.
[42] T. Basak, G. Aravind, S. Roy, A. Balakrishnan, Heatline analysis of heat recovery and thermal transport in materials confined within triangular cavities, Int. J. Heat Mass Transf. 53 (2010) 3615–3628.
[43] P. Colella, E. Puckett, Modern Numerical Methods for Fluid Flow, University of California, California, USA, 1994.